stimulation of human peripheral blood mononuclear cells with viruses has revealed that plasmacytoid dendritic cells (pDCs), a rare subset of dendritic cells (DCs), are the major producer of type I IFNs (Cella et al., 1999; Siegal et al., 1999). Subsequently, a mouse counterpart of human pDC was identified based on the surface expression of CD11c and B220 (Asselin-Paturel et al., 2001; Bjorck, 2001; Nakano et al., 2001). It has been shown by ex vivo experiments that the TLR system is responsible for the secretion of type I IFNs in pDCs (Kato et al., 2005). pDCs produced IFN-α irrespective of the presence of type I IFN receptor (Barchet et al., 2002; Prakash et al., 2005). In contrast, conventional DCs (cDCs) and fibroblasts produce type I IFNs in response to viral infection in vitro in a RLH-dependent fashion (Diebold et al., 2003; Kato et al., 2005). These cell types produce IFN-α via type I IFN receptor-mediated positive feedback. IFN-producing killer dendritic cells (IKDCs) are also reported to produce type I IFNs (Chan et al., 2006; Taieb et al., 2006), although this has been questioned in a recent report (Vremec et al., 2007). However, the contribution of each cell type to the production of type I IFNs in vivo remains to be determined. Additionally, the in vivo role of the two abovementioned viral detector systems in the production of type I IFNs is unknown.

Currently used methods have not succeeded in monitoring the expression of type I IFNs in vivo. For instance, enzyme-linked immunosorbent assay (ELISA) is not suitable for detecting type I IFNs at a single-cell level. Although intracellular staining of IFN-α is sensitive enough to detect IFN-α expression in ex vivo experiments, it is difficult to monitor IFN-α-producing cells in vivo. Therefore, we generated a reporter mouse strain in which the coding sequence of the *Ifna6* gene was replaced by the GFP coding sequence. Comparison between GFP expression and intracellular IFN-α staining, and quantitative real-time PCR (Q-PCR) analysis for the expression of multiple IFN-α genes in GFP^+ cells, revealed that this reporter recapitulated the expression of various IFN-α genes. pDCs were the sole producer of IFN-α in response to TLR7 and TLR9 ligand inoculation, whereas cDCs were the main producer in response to poly (I:C), the TLR3-MDA5 ligand. In response to systemic RNA virus infection, not only pDCs, but also cDCs, macrophages, and monocytes, produced IFN-α. The TLR system was responsible for the production of IFN-α in pDCs, whereas cDCs and macrophages utilized the RLH system. When the same virus was introduced intranasally, the IFN-α-producing cells shifted from pDCs to alveolar macrophages (AMs) and cDCs. Depletion of AMs increased the virus yield after NDV infection, further supporting the role of this cell type in the control of viral infection. Production of IFNs in AMs and cDCs depended on the RLH system, whereas IPS-1 deficiency led to IFN-α production in pDCs. Our data clearly demonstrates that distinct IFN-producing cells (IPCs) are activated in a tissue-specific manner. This serves to emphasize the importance of local antiviral cells in the natural course of the response to infection.

RESULTS

Generation of *Ifna6^{gfp}* Knockin Locus and Its Validation In Vitro

To investigate which cell population or populations produce IFN-α in vivo, we generated a mouse strain in which the coding sequence of the *Ifna6* gene was replaced by the GFP coding sequence (Figures 1A and 1B). Among multiple IFN-αs, we chose IFN-α6 because IFN-α6 expression is strongly induced in response to viral infection in various cell types in vitro, as detected by Q-PCR and DNA microarray analysis (Matsui et al., 2006). Additionally, IFN-α6 was reported to be regulated solely by IRF-7, as is the case for various IFN-αs, except for IFN-α4; IFN-β and IFN-α4 are reported to be regulated by IRF-3 in addition to IRF-7 (Honda et al., 2005). In the targeted allele, the GFP coding sequence and *loxP*-flanked neomycin-resistance cassette replaced the complete sequence encoding IFN-α6. The neomycin-resistance cassette was excised in targeted embryonic stem (ES) cells in vitro by transfecting a plasmid containing the Cre recombinase coding gene. The resulting allele *Ifna6^{gfp}* produced GFP instead of IFN-α6. We used mice heterozygous for *Ifna6^{gfp}* to circumvent the interference in IFN-α6 production.

We first examined whether the *Ifna6^{gfp}* allele recapitulated IFN-α expression in vitro. Flt3L-induced bone marrow DCs (Flt3L-BMDCs) prepared from *Ifna6$^{gfp/+}$* mice were infected with Newcastle disease virus (NDV) for 6 hr, and intracellular IFN-α staining was performed (Figure 1C). Flow cytometry analysis revealed that the number of GFP-positive $CD11c^+B220^+$ pDCs markedly increased in infected cells, and most of the intracellular IFN-α-positive cells were also positive for GFP. Next, GFP-positive (GFP^+) and GFP-negative (GFP^-) pDCs were FACS-sorted after NDV infection. The expression of type I IFN genes was then examined by Q-PCR (Figure 1D). Expression of the *Ifna6*, *Ifna2*, *Ifna4*, and *Ifna5* genes, as well as the *Ifnb1* gene, in GFP^+ cells was markedly augmented, being about ten times higher than that in GFP^- cells. By contrast, the expression of the *Cxcl10* gene was almost equally upregulated in both GFP^+ and GFP^- cells. This result indicates that the expression of GFP reflects the induction of IFN-αs and IFN-β, but not the general transcriptional upregulation invoked by NDV infection. Production of IFN-α was not altered between *Ifna6$^{+/+}$* and *Ifna6$^{gfp/+}$* cells. This indicated that the heterozygous *Ifna6^{gfp}* allele does not affect IFN-α production overall (Figure 1E). Taken as a whole, these results showed that the expression of GFP in *Ifna6$^{gfp/+}$* cells is an appropriate reporter for IFN-α production in vitro.

IPCs in Response to TLR Ligand Stimulation In Vivo

We next examined the responses of *Ifna6^{gfp}* mice to TLR and RLH ligands in vivo. Systemic administration of synthetic nucleotide analogs, such as D-type CpG-oligodeoxynucleotide (CpG-ODN) (a ligand for TLR9), R-848 (TLR7), and poly (I:C) (TLR3-MDA5), are known to induce IFN-α production in vivo (Asselin-Paturel et al., 2005; Hemmi et al., 2002; Kato et al., 2006). CpG-ODN was administered in *Ifna6$^{gfp/+}$* mice and GFP expression was

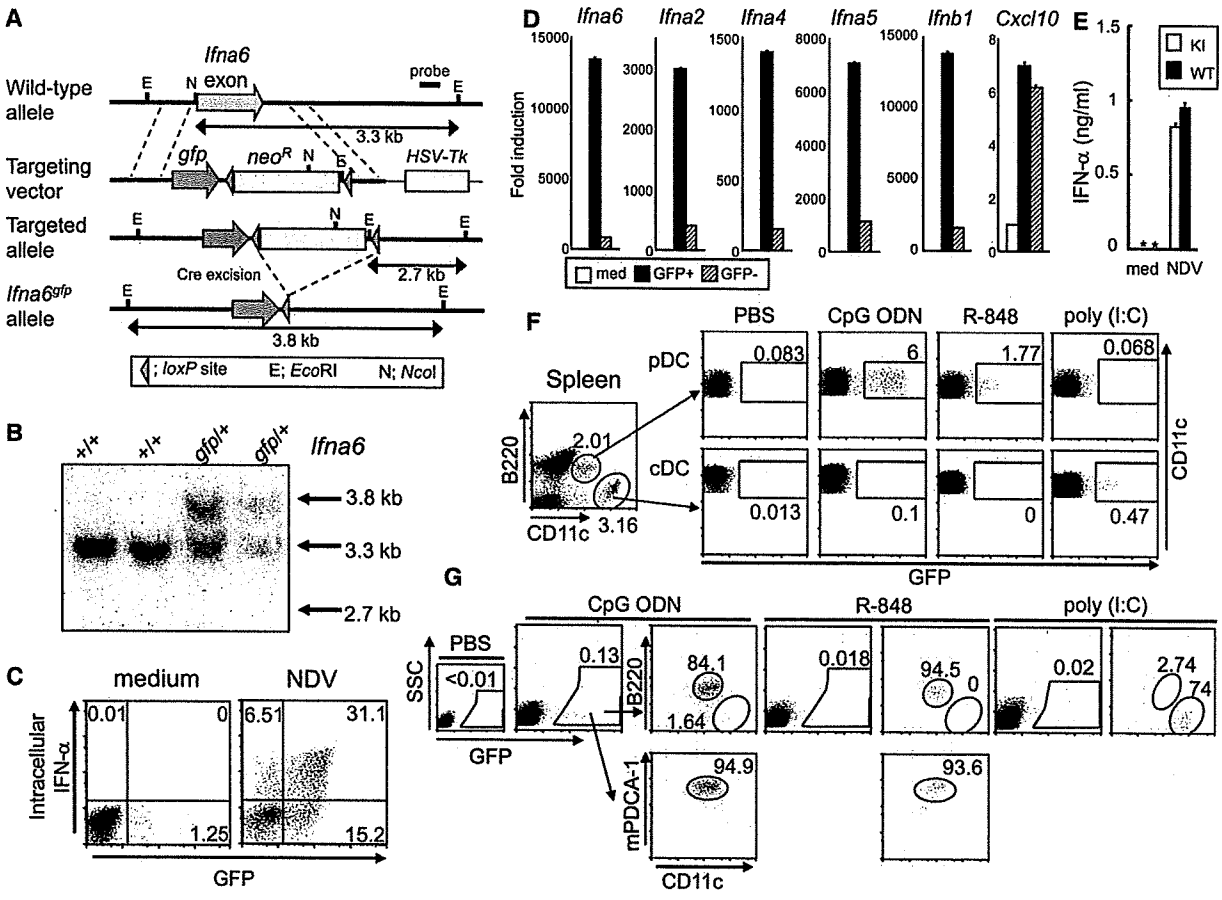

Figure 1. Generation of *Ifna6*^{gfp} Knockin Mice

(A) *Ifna6* gene and its flanking region ("wild-type allele") were used for creating the targeting vector ("targeting vector"). The resulting allele contains both *gfp* and *neo* genes ("targeted allele"). Excision of the *neo* gene by Cre recombinase resulted in the final mutated allele ("*Ifna6*^{gfp} allele") in which the *gfp* gene totally replaces the IFN-α6 coding sequence.

(B) Homologous recombination and excision of the *neo* gene was verified by Southern blot analysis.

(C) FACS plots of intracellular IFN-α (vertical) versus GFP (horizontal) staining obtained from untreated ("medium") and NDV-infected ("NDV"), Flt3L-induced, BM-derived pDCs. The data are representative of three independent experiments.

(D) GFP$^+$ cells were sorted from NDV-infected Flt3L-BMDCs, and amounts of mRNA for indicated IFN-α subtypes and other genes were quantified by quantitative real-time PCR (Q-PCR). Mean relative expressions against untreated cells are shown with standard error. Open histogram, untreated; closed, NDV-infected GFP$^+$ cells; shaded, NDV-infected GFP$^-$ cells.

(E) IFN-α concentrations in culture supernatants of NDV-infected ("NDV") or uninfected ("med") Flt3L-BMDC from *Ifna6*$^{+/+}$ and *Ifna6*$^{gfp/+}$ mice were determined by ELISA. The concentration of IFN-α is shown with standard error.

(F and G) Detection of IFN-α6-producing cells in vivo. PBS and D35/DOTAP complex (CpG) or R-848 was intravenously administered into *Ifna6*$^{gfp/+}$ mice. Four or two hours after inoculation of CpG-ODN or R-848, respectively, whole splenocytes were prepared, stained with CD11c and B220, and analyzed by FACS. pDCs and cDCs were gated and GFP expression was assessed (F). Conversely, GFP$^+$ cells were selected and analyzed for the expression of CD11c and B220 or mPDCA-1 (G). Numbers shown in each plots indicate the ratio of gated cells to total cells in the plot. The data are representative of three independent experiments.

examined in the lymphoid organs 4 hr after administration. Splenocytes most frequently contained GFP$^+$ cells, whereas cells from lymph nodes (LNs) and bone marrow (BM) were rarely GFP$^+$. In the spleen, CD11c^{int}B220$^+$ pDCs, but not CD11c^{hi} cDCs, DX5$^+$ IKDCs, or other lymphocytes, contained GFP$^+$ cells (Figure 1F and data not shown). In turn, most GFP$^+$ splenocytes expressed CD11c, B220, and mPDCA-1, indicating that pDCs are the predominant IPCs (Figure 1G). R-848 was also found to induce IFN-α production exclusively in pDCs 2 hr after inoculation (Figures 1F and 1G). Therefore, we concluded that pDCs are the sole IPC upon TLR7 and TLR9 stimulation in vivo. Of note, however, intravenous inoculation of poly (I:C) led to the increase of GFP$^+$ cDCs, but not pDCs, in the spleen (Figures 1F and 1G).

Determination of IPCs in Response to Systemic RNA Virus Infection In Vivo

FACS analysis of splenocytes from *Ifna6*$^{gfp/+}$ mice intravenously administered NDV revealed that pDCs, CD11c^{hi}B220$^-$ cDCs, and CD11c$^-$Mac1$^+$F4/80$^+$ macrophages contained GFP$^+$ cells (Figure 2A and Figure S3 in

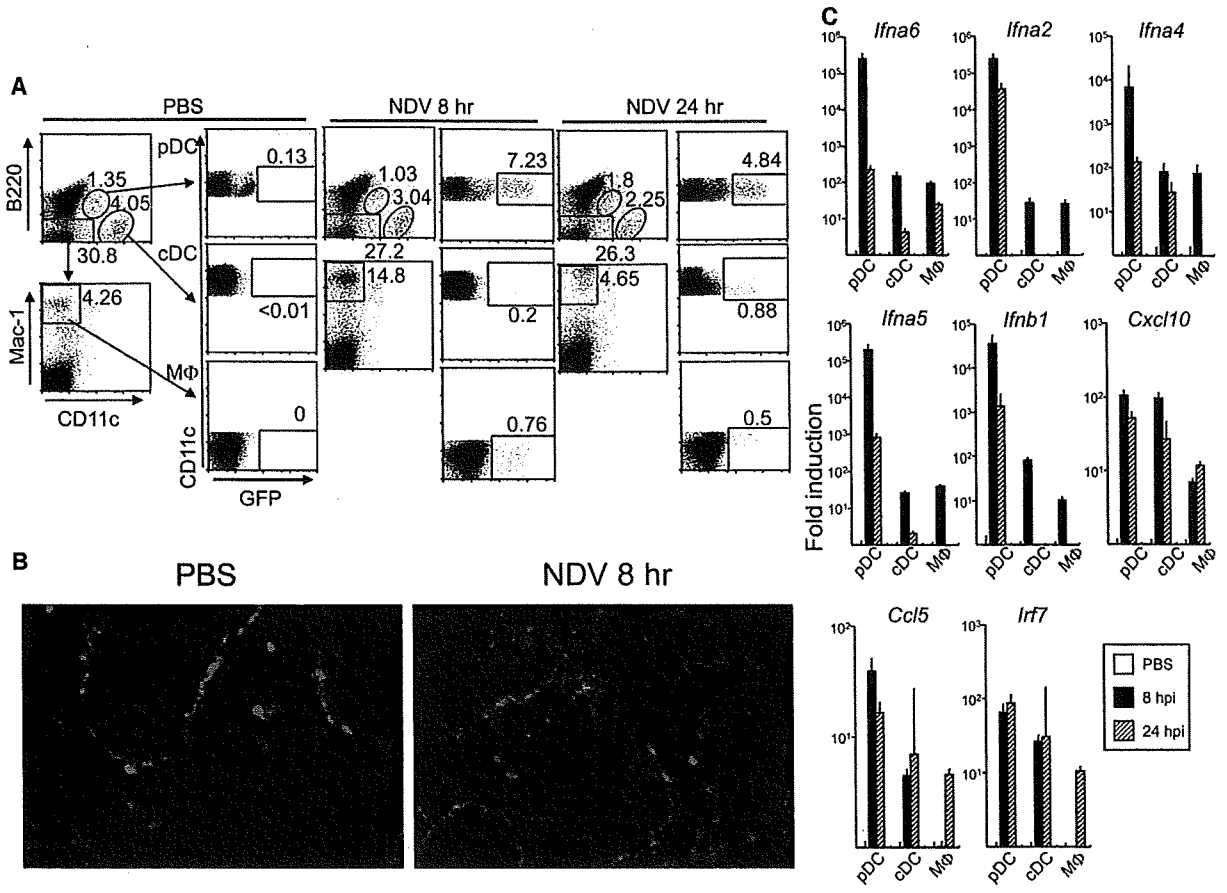

Figure 2. Identification of IPCs in Response to Systemic NDV Virus Infection

(A) NDV (1×10^7 pfu) was administered intravenously, and whole splenic cells were prepared 8 and 24 hr after infection. The expression of GFP in pDCs ($CD11c^{int}B220^+$), cDCs ($CD11c^+B220^-$), and macrophages ($Mac\text{-}1^+CD11c^-$) was analyzed. The data are representative of five independent experiments with similar results.

(B) Localization of GFP^+ cells in spleen. Cryosections of spleen from PBS- or NDV-treated mouse were stained with anti-GFP (green) and anti-MAdCAM-1 (red) as in Experimental Procedures.

(C) mRNA prepared from pDCs, cDCs, and macrophages (MΦ) obtained from NDV-infected or uninfected mice were subjected to Q-PCR. Fold induction of each mRNA type normalized to cells from PBS-treated mice is shown as mean with standard error (n = 2). Open bar, PBS; closed, 8 hr after infection; shaded, 24 hr after infection.

the Supplemental Data available with this article online). Four percent to eight percent of pDCs were GFP^+, whereas less than one percent of cDCs and macrophages were GFP^+. Nevertheless, when GFP^+ cells were collected and examined for their surface markers, cDCs and macrophages constituted more than 30% of GFP^+ cells at 8 hr after infection, indicating that these cell types occupied a substantial percentage of IFN-α producers (Figure S1A). This is because cDCs and macrophages constituted about 5% of total splenocytes, whereas around 1% of splenocytes were pDCs. Immunofluorescent microscopy revealed that GFP^+ cells localized at the marginal zone (MZ), outside of the marginal sinus stained with anti-MAdCAM-1 (Figure 2B).

Next, we sorted pDCs, cDCs, and macrophages from splenocytes of untreated or NDV-infected mice. The expression of IFN-α and chemokine genes was then determined by Q-PCR. Expression of the genes encoding IFN-α2, IFN-α4, IFN-α5, and IFN-α6 was strongly upregulated in pDCs, cDCs, and macrophages, although to a lesser extent in the latter two (Figure 2C). This result indicated that the production of IFN-α6 is representative of the production of various IFN-α subtypes, even in vivo.

In the peripheral blood, $Mac\text{-}1^+CD11c^-$ monocytes and macrophages contained GFP^+ cells at 8 hr after infection (Figure S1B). Additionally, $Mac\text{-}1^+CD11c^-$ monocytes and macrophages in the liver and BM also contained GFP^+ cells at 8 and 24 hr after injection (Figure S2). In BM, GFP^+ pDCs were also found. However, the frequency of GFP^+ cells in these organs was much lower than that in the spleen, indicating that the spleen is the organ which responds to systemic viral infection most efficiently. A vesicular stomatitis virus NCP mutant (VSV-NCP) also induced GFP expression in pDCs, cDCs, and macrophages in spleen, but hardly so in BM, LN, and liver (Figure S4 and data not shown).

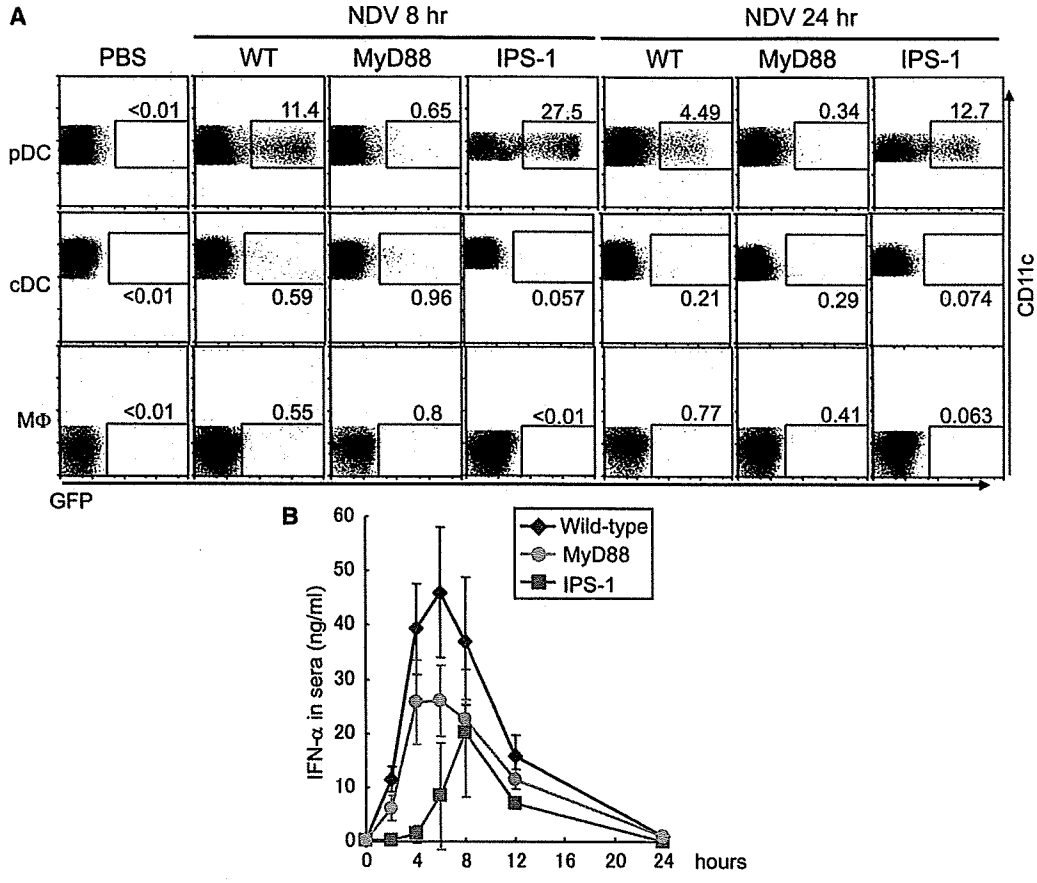

Figure 3. Differential Involvement of Signaling Pathways in IFN-α Production

(A) *Ifna6*$^{gfp/+}$ mice with wild-type ("WT"), MyD88-deficient ("MyD88"), or IPS-1-deficient ("IPS-1") backgrounds were infected with NDV and splenocytes were analyzed for the expression of GFP using FACS at the indicated time points. The data are representative of three independent experiments.

(B) IFN-α concentrations in sera from NDV-infected wild-type (diamond, green), MyD88-deficient (circle, orange), and IPS-1-deficient (rectangle, blue) mice were measured by ELISA. The mean value with standard error is shown (n = 3).

Collectively, these data indicate that upon systemic viral infection, splenic pDC, as well as cDC, monocytes, and macrophages in spleen and other organs, produced IFN-α.

Contribution of Intracellular Signaling Molecules to the Activation of IPCs In Vivo

We previously showed that the TLR and RLH pathways are important for the induction of IFN-α in pDCs and cDCs, respectively, by examining the production of IFNs in cDCs and pDCs ex vivo (Kato et al., 2005). However, it was not clear whether these pathways operate in a similar manner in vivo. When *Ifna6*$^{gfp/+}$ mice lacking MyD88 were infected with NDV, GFP$^+$ pDCs were severely decreased in number compared with those in wild-type mice (Figure 3A). In contrast, the number of GFP$^+$ cDCs and macrophages was not altered in MyD88-deficient mice, confirming that the TLR pathway mediates IFN-α induction in pDCs in vivo. In IPS-1-deficient mice, the increase of the GFP$^+$ cell number in cDCs and macrophages, but not in pDCs, was abrogated, showing that cDCs and macrophages utilize the RLH pathway in vivo (Figure 3A).

We then examined the concentration of IFN-α in the sera of NDV-infected wild-type, MyD88-deficient, and IPS-1-deficient mice. As shown in Figure 3B, production of IFN-α was partially impaired in both MyD88-deficient and IPS-1-deficient mice compared with wild-type controls. Interestingly, in the case of IPS-1-deficient mice, more severe impairment of IFN-α production was observed from 2 to 6 hr after infection than at later time points. This result showed that cells utilizing the RLH pathway, such as cDCs, monocytes, and macrophages, contribute to production of IFN-α serum at the initial stage of systemic viral infection.

Thus, consistent with former reports, cDCs and pDCs produce IFN-α via the RLH pathway and the TLR pathway, respectively.

Identification of IPCs in Response to Local Viral Infection of the Lung

In the natural course of viral infection, viruses do not directly enter the blood stream, but attack mucosal surfaces to invade the host. It remains to be clarified whether the same cell types are responsible for type I IFN production in

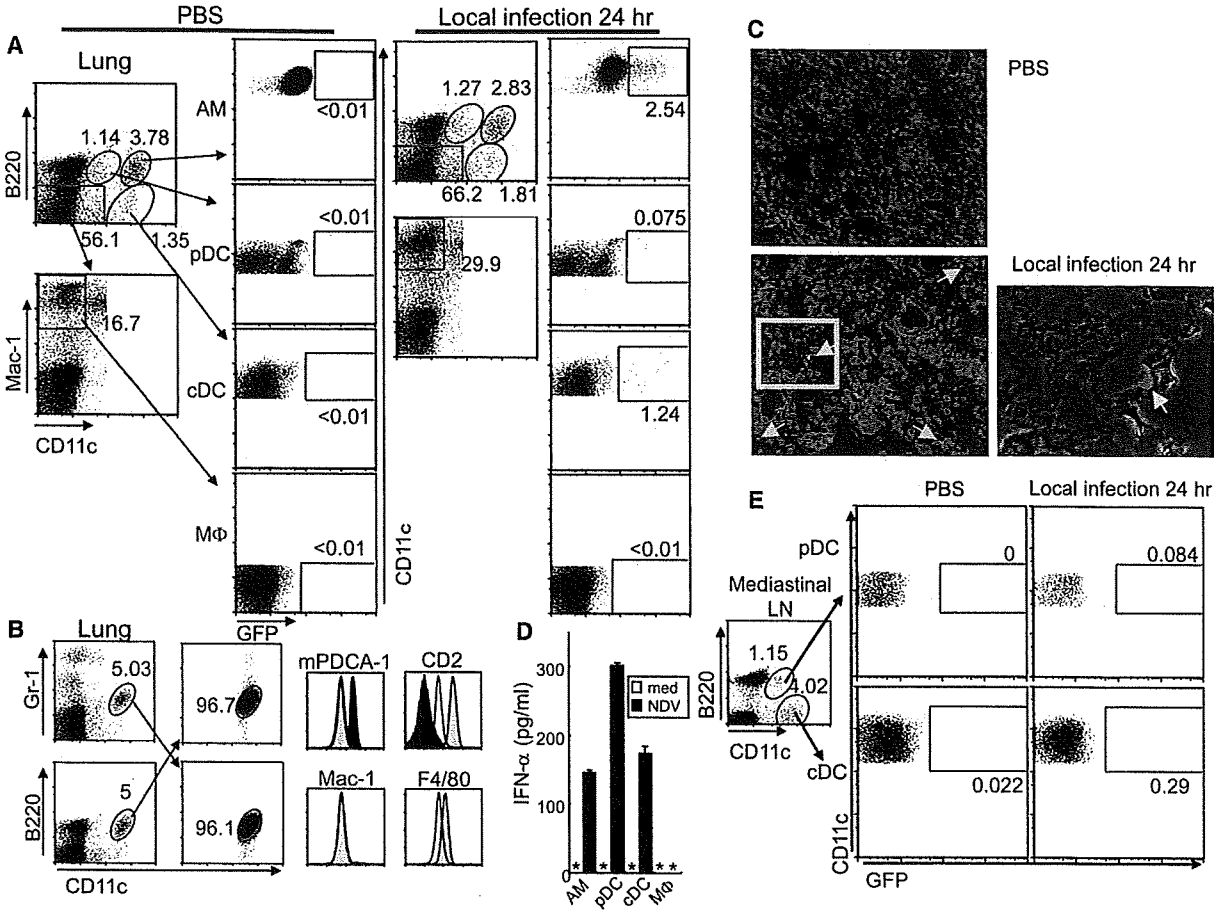

Figure 4. Identification of Alveolar Macrophages as Lung-Local IPCs

(A) *Ifna6*^{gfp} mice were intranasally administered PBS or NDV. Twenty-four hours after infection, lung cells were isolated as in Experimental Procedures and subjected to FACS analysis. AM, alveolar macrophage. Others are the same as in Figure 2A. The data are representative of four independent experiments with similar results.

(B) Lung cells from a mouse were stained and subjected to FACS analysis. In the upper two dot plots, expression of Gr-1 (vertical) versus CD11c (horizontal) is shown. In the bottom two dot plots, expression of B220 (vertical) versus CD11c (horizontal) is shown. Gated cells in the left two panels were expanded and the plots are shown in the right two panels. Histograms represent the expression of each of the surface molecules on cells gated in a B220 versus CD11c plot. Open histogram, unstained control; shaded, stained with indicated antibodies. Solid histograms in mPDCA-1 and CD2 indicate fluorescence intensities of the surface molecules on pDCs and cDCs, respectively. Data shown are representative of two mice.

(C) Lung lobes from an *Ifna6*$^{gfp/+}$ mouse infected intranasally with NDV for 24 hr were analyzed by immunofluorescence. Overlay images of phase contrast images, with DAPI-stained nucleus in blue and GFP in green, are shown. GFP$^+$ cells are indicated by yellow arrows. Upper panel, PBS-treated lung image; lower left panel, NDV-infected lung; lower right panel, magnified image of the region that corresponds to the yellow box in the lower left image.

(D) IFN-α production by sorted AMs, pDCs, cDCs, and MΦs from lung in vitro. FACS sorted cells, as described in Experimental Procedures, were infected with NDV or left uninfected. The culture supernatants were collected and subjected to ELISA at 24 hr after infection. The data shown are mean concentrations with standard errors. Asterisk, not detected.

(E) Mediastinal LNs from *Ifna6*$^{gfp/+}$ mice uninfected or intranasally infected with NDV for 24 hr were isolated and subjected to FACS analysis. The data are representative of three independent experiments.

response to systemic and local viral infection. To answer this question, we applied an intranasal infection model to *Ifna6*$^{gfp/+}$ mice. When the mice were infected intranasally with NDV, CD11c^{int}B220$^+$ pDCs did not contain a GFP$^+$ population, in contrast to the group undergoing systemic infection (Figure 4A). Also, neither Mac-1$^+$CD11c$^-$ monocytes and macrophages nor lymphocytes contained GFP$^+$ cells (Figure 4A and data not shown). cDCs showed modest but relevant increases in the induction of GFP$^+$ cells. Further, a CD11c^{hi} population was found to highly increase the number of GFP$^+$ cells (Figure 4A, AM). These CD11c$^+$GFP$^+$ cells showed high autofluorescence and the expression of B220 was comparable to that in the control staining. This indicated that this population did not express B220 (Figure S5). These cells were also negative for Mac-1, CD8a, and Gr-1, but positive for F4/80 and CD2 (LFA-2). This population was found to be identical to previously reported AMs (Figure 4B) (de Heer et al., 2004).

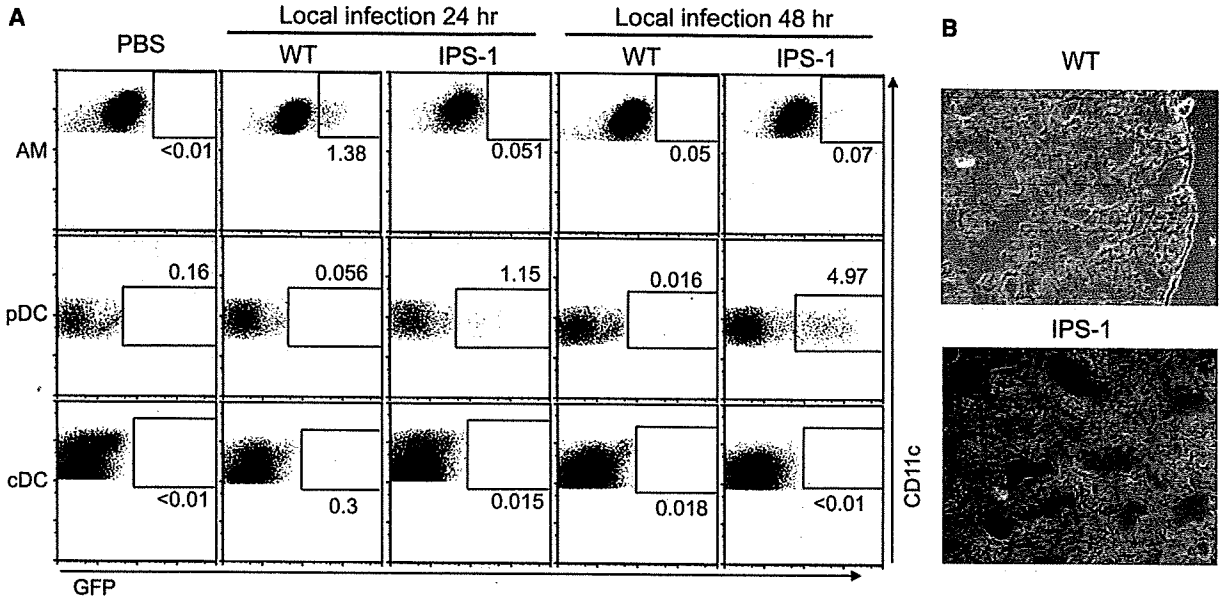

Figure 5. Effect of IPS-1 Deficiency on IFN-α Production in Lung

(A) Wild-type or IPS-1-deficient *Ifna6*$^{gfp/+}$ mice were infected intranasally with NDV, and lung cells were analyzed using FACS at the indicated time points. AMs, pDCs, and cDCs were gated as in Figure 4A. The data are representative of two independent experiments with essentially identical results.

(B) Immunofluorescence images of lung sections from wild-type mice (upper) or IPS-1-deficient *Ifna6*$^{gfp/+}$ mice (lower) are shown as in Figure 4C.

More than 80% of GFP$^+$ lung cells belonged to this cell population (Figure S5). Consistent with these observations, a histological examination revealed that most GFP$^+$ cells were localized at alveoli (Figure 4C). To verify IFN-α production from these populations, pDC, cDC, macrophage, and CD11c^{hi}CD2^{hi} AM populations were FACS-sorted and stimulated by NDV in vitro. The AMs, cDCs, and pDCs, but not Mac1$^+$CD11c$^-$ macrophages, produced comparable amounts of IFN-α in response to NDV (Figure 4D).

Lung viral infection is likely to influence mediastinal LNs. We found that cDCs contained GFP$^+$ cells in the mediastinal LN 24 hr after intranasal infection, whereas GFP$^+$ pDCs were not found (Figure 4E and data not shown). This observation suggested that virus infection in the lung induces IFN-α production in the LN by cDCs, which might have migrated from the lung.

In summary, AMs and cDCs, but not pDCs, are IFN-α-producing cells after pulmonary infection with NDV.

Role of the RLH Pathway in the Production of IFN-α in AMs

To elucidate the mechanism of virus-mediated IFN-α production in the lung, IPS-1-deficient *Ifna6*$^{gfp/+}$ mice were infected intranasally with NDV. IPS-1 deficiency abrogated induction of GFP$^+$ cells in both AMs and cDCs (Figure 5A). Interestingly, the number of GFP$^+$ pDCs was highly increased at 48 hr after infection in IPS-1-deficient mice, suggesting that the IPS-1 deficiency resulted in the failure of initial antiviral responses in AMs and cDCs, and led to massive production of IFN-α by pDCs. Further histological examination revealed that GFP$^+$ cells in IPS-1-deficient mice infected with NDV were localized in the interstitium between alveoli (Figure 5B). This result further confirmed the production of IFN-α from pDCs in the absence of IPS-1, because pDCs are localized in the interstitium (de Heer et al., 2004). In contrast, a MyD88 deficiency did not affect the frequency of GFP$^+$ AMs and cDCs (data not shown), indicating that AMs and cDCs rely on the RLH system to produce IFN-α.

Functional Role of AMs in Antiviral Responses In Vivo

Although DCs are reported to play an important role in antiviral responses, the role of AMs is unclear. To examine the role of AMs in antiviral responses, we tried to deplete AMs using liposome-encapsulated dichloromethylene bisphosphonate (Cl_2MBP-liposome). Consistent with previous reports (Thepen et al., 1989), intranasal treatment of mice with Cl_2MBP-liposome, but not PBS-liposome, led to specific depletion of the CD11c^{hi}CD2^{hi} AM population 24 hr after treatment without altering the population of cDCs, pDCs, and macrophages (Figure S6). When Cl_2MBP-liposome-treated *Ifna6*$^{gfp/+}$ mice were further infected intranasally with NDV, GFP$^+$ cells in lung pDCs increased in number, implying that impaired initial responses to NDV activated pDCs (Figure 6A). Neither the depletion of AM nor the IPS-1 deficiency markedly affected IFN-α concentration in sera 24 hr after infection, suggesting that pDCs compensated for the IFN-α production from the decreased number of AMs (Figure 6B). Histological examination of AM-depleted mice revealed that

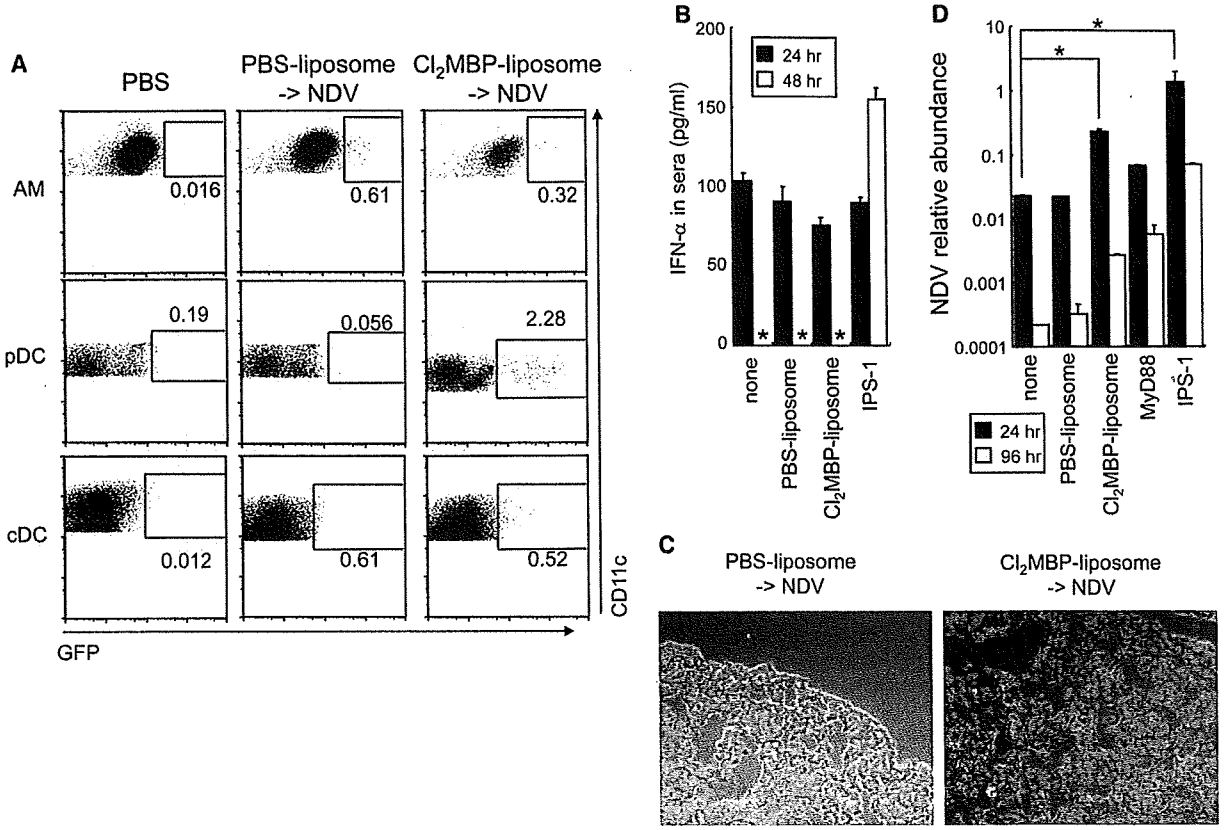

Figure 6. Effect of Depletion of AMs on Antiviral Responses in Lung

(A) AMs were depleted or left undepleted by intranasal instillation of Cl_2MBP-lipsome or PBS-liposome, respectively. Twenty-four hours after instillation, mice were infected with NDV for another twenty-four hours. Lungs were collected and GFP expression in AMs, pDCs, and cDCs was assessed using FACS.

(B) IFN-α levels in sera 24 or 48 hr after intranasal infection with NDV were measured by ELISA. Asterisks, not detected.

(C) Immunofluorescence images of lung from PBS-liposome-treated mice (left) or Cl_2MBP-lipsome-treated mice (right) are shown as in Figure 4C.

(D) The abundance of NDV in lung was quantified by Q-PCR for NDV nucleoprotein mRNA. Data shown are the mean value with standard error (n = 2). *$p < 0.05$ with two-sided Student's t test. All the data in this panel are representative of at least two independent experiments with essentially identical results.

GFP^+ cells were mainly localized in the interstitium of the lung (Figure 6C).

Next we examined the role of AMs in the clearance of infected NDV in the lung by measuring the expression of mRNA encoding NDV nucleocapsid protein with Q-PCR. The expression of NDV nucleoprotein was observed in untreated or PBS-liposome-treated mice 24 hr after infection, and decreased less than 1% from 24 hr to 96 hr after infection (Figure 6D). In contrast, the expression of the NDV nucleoprotein gene was around 10 times higher in AM-depleted mice than in control mice at 24 and 96 hr after infection, indicating that AMs play a critical role in the clearance of NDV infection. When we examined whether deficiency of MyD88 or IPS-1 influenced virus clearance, IPS-1-deficient mice exhibited a much higher NDV burden compared with MyD88-deficient mice, although MyD88-deficient mice showed a modest increase in the expression of the NDV nucleoprotein (Figure 6D). This result indicated that in the acute phase of infection, the RLH system plays a more important role in the elimination of lung viral infection than the TLR system does. These results underlined the importance of AMs in the initial elimination of invading viruses.

Subversion of AM-Mediated IFN-α Production by Wild-Type Sendai Virus

We next investigated whether other RNA viruses also induce IFN-α production in AMs. We used Sendai virus (SeV), a pathogenic virus widely used as a respiratory viral infection model in mice (Woodland et al., 2001), and VSV. When AMs and pDCs were purified from the lung and stimulated with viruses, AMs produced IFN-α in response to VSV-NCP and SeV with mutated C proteins (SeV Cm), as well as NDV (Figure 7A). However, AMs failed to produce IFN-α in response to wild-type SeV. In contrast, pDCs produced IFN-α in vitro in response to all the viruses tested. It has been shown that SeV C proteins suppress host IFN responses (Kato et al., 2007), and these results suggested that SeV inhibited IFN-α production in AMs, but not pDCs, by C proteins. When wild-type SeV was

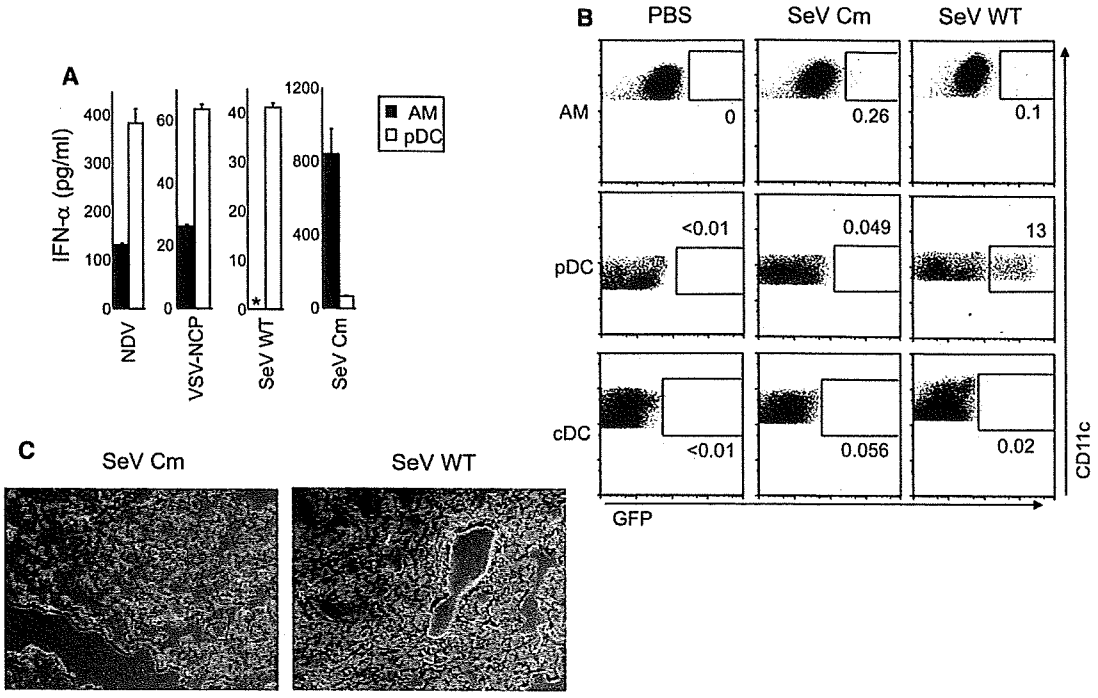

Figure 7. Subversion of AM-Mediated or cDC-Mediated Antiviral Responses, or Subversion of Both, by Sendai Virus

(A) In vitro IFN-α production by AMs and pDCs in response to various viruses. AMs and pDCs were sorted and infected in vitro for 24 hr. IFN-α concentrations in the culture supernatants were measured with ELISA. Asterisk, not detected.

(B) GFP expressions in AMs, pDCs, and cDCs were analyzed at 24 hr after intranasal infection with wild-type Sendai virus (SeV WT) or its mutant, SeV Cm.

(C) Immunofluorescence images of lung infected with SeV Cm (left panel) or SeV WT (right) are shown. The data are representative of two independent experiments with same results.

introduced intravenously, the virus induced IFN-α production from pDCs, but not from cDCs or macrophages (Figure S7).

Thus, we investigated IPCs in the lung in response to SeV Cm and wild-type SeV infection. As expected, SeV Cm, as well as NDV, induced IFN-α production from AMs, but not from pDCs (Figure 7B). In sharp contrast, the number of GFP$^+$ pDCs, but not cDCs and AMs, was highly increased in response to intranasal wild-type SeV infection, resembling the result obtained in AM-depleted and IPS-1-deficient mice (Figure 7B). This was further confirmed by immunofluorescence images of the lung infected with SeV, which showed the presence of GFP$^+$ cells in the interstitium (Figure 7C). In contrast, SeV Cm induced GFP expression in AMs. These results suggested that SeV targets AMs for suppressing IFN-α production, and that the subversion is essential for SeV virulence. Collectively, these data emphasized the importance of the first-line antiviral responses mediated by AMs.

DISCUSSION

In this study, we generated an *Ifna6^{gfp}* knockin allele in which the expression of GFP is induced under the control of the *Ifna6* promoter. Validation analysis showed that this allele recapitulated IFN-αs and IFN-β expression in response to viral infection both in vitro and in vivo. IFN-α6 is a subtype of IFN-αs whose expression is reported to be controlled by IRF-7 and induced by viral, but not bacterial, infections. In contrast, IFN-β is regulated by IRF-3 in addition to IRF-7 (Honda et al., 2005), and it is induced by both viral and bacterial components. However, an expression analysis of IFN-α2, IFN-α4, IFN-α5, and IFN-β mRNA in GFP$^+$ pDCs revealed that IFN-α6-producing cells also expressed other subtypes of IFN-α and IFN-β in response to NDV stimulation, indicating that expression of GFP recapitulates not only the expression of the *Ifna6* gene but also expressions of various IFN-α and IFN-β genes regardless of the subtypes. Thus, *Ifna6$^{gfp/+}$* mice are an appropriate reporter strain for analysis of type I IFN production, although it is not proven if type I IFNs are coregulated in response to various stimuli.

By intravenously treating *Ifna6$^{gfp/+}$* mice with NDV, we found that pDCs, cDCs, and macrophages in the spleen, monocytes and macrophages in peripheral blood, and (to a lesser degree) monocytes and macrophages in liver and BM were responsible for the production of type I IFNs. In accordance with previous observations, MyD88 was critical for the increase in GFP$^+$ pDCs, whereas IPS-1 was essential for the appearance of other GFP$^+$ cells such as cDCs and macrophages (Kato et al., 2005). It is unexpected that monocytes and macrophages consist

of a large portion of IPCs in vivo. Because the RLH system is essential for IFN-α production in this cell type, monocytes and macrophages seem to be actually infected. Impaired production of serum IFN-α in IPS-1-deficient mice also implies the importance of non-pDCs in virus-induced IFN-α production. Our data indicated that cell types other than pDCs also make a large contribution to type I IFN production during systemic viral infections.

The IPS-1-dependent pathway contributes substantially to increases in serum IFN-α at an early time point after infection with NDV, although the MyD88-dependent pathways are also critical at later time points. Accordingly, about 30% of GFP$^+$ splenocytes were macrophages and cDCs at 8 hr after NDV infection, but the ratio dropped to below 10% at 24 hr. In the spleen of NDV-infected *Ifna6^{gfp}* mice, GFP$^+$ cells were localized at the MZ. This is consistent with previous reports that used an IFN-α antibody to show that IPCs are localized at the MZ (Asselin-Paturel et al., 2005; Dalod et al., 2002). Upon systemic NDV infection, GFP$^+$ cells were almost exclusively found in the spleen, though quite a few GFP$^+$ pDCs were observed in other lymphatic organs, such as BM and LNs. VSV and SeV also induced GFP expression mostly in the spleen, indicating that the spleen is the most important organ for the production of type I IFNs in response to blood-borne viruses. Because the MZ is important for sequestering blood-borne pathogens, and mice with abnormal MZ organization failed to mount proper IFN-α production in response to viral infection (Louten et al., 2006), IPCs activated by systemic NDV infection are probably localized in the splenic MZ. pDCs are mostly localized in the T cell area and in the red pulp, but rarely localize in the MZ although they migrate to the MZ to form clusters in response to CpG-DNA stimulation (Asselin-Paturel et al., 2005). In contrast, cDCs originally localize in the MZ. Thus, it is possible that invading NDV encounters macrophages and cDCs at the MZ first, and then pDCs that have migrated to the MZ. Although further detailed analysis of localization and time-course changes needs to be addressed, this may explain the temporal differences in the contributions of IPS-1- and MyD88-dependent pathways in the production of IFN-α.

In contrast to systemic virus infection, intranasal treatment of *Ifna6^{gfp}* mice with NDV failed to increase the number of GFP$^+$ cells in pDCs. By characterizing GFP$^+$ cells upon intranasal infection, we identified AMs and cDCs, particularly AMs, as the major IFN-α producers. AMs are reported to sample and respond to microorganisms that have entered the alveolar space. They phagocytose invading bacteria and evoke inflammation by producing proinflammatory cytokines (Peters-Golden, 2004). They are also reported to phagocytose virus-infected apoptotic cells (Hashimoto et al., 2007). However, our results suggested that direct infection of AMs with viruses is required for the production of IFN-α. The role of AMs in the clearance of viral infection was also demonstrated by the consequences of the depletion of AMs. Thus, AMs function as sentinels, recognizing infectious viruses and alerting surrounding cells. AMs do not seem to migrate to mediastinal LNs even after viral infection, suggesting that type I IFNs produced by AMs activate surrounding cells in an autocrine or paracrine manner to prepare for any virus infection. Taken together, our data highlighted the importance of the initial production of IFN-α and the elimination of invading viruses by AMs.

cDCs, but not pDCs, produced IFN-α in response to local infection in mediastinal LNs. Because GFP$^+$ cDCs were also found in lung tissue, it is possible that cDCs activated in the lung tissue are migrating to mediastinal LNs. Given the function of type I IFNs in the activation of acquired immune responses (Stetson and Medzhitov, 2006), the major role of cDCs may be to activate T cells in LNs rather than function as local IPCs.

Earlier reports indicated that pDCs produce type I IFNs to help elicit the acquired immune response (Yoneyama et al., 2005), although we failed to detect GFP$^+$ pDCs in response to intranasal NDV infection in *Ifna6^{gfp}* mice. However, massive amounts of GFP$^+$ pDCs were detected either when AMs were depleted or in the absence of IPS-1. These results suggested that pDCs start to function when AM- and cDC-mediated host defense mechanisms are impaired, and that pDCs may function as the backup system to achieve robust antiviral IFN-α production.

Wild-type SeV is reported to repress host antiviral responses mainly by inhibiting type I IFN signaling via C proteins; this activity is essential for the pathogenicity of the virus (Kato et al., 2007). In vitro experiments showed that wild-type SeV did not induce IFN-α production in AMs, whereas SeV Cm highly induced IFN-α. Upon local lung infection with wild-type SeV, AMs and cDCs did not appear to contain GFP$^+$ cells, indicating that AMs and cDCs failed to produce IFN-α. This result indicates that SeV has a sophisticated mechanism or mechanisms to subvert host antiviral response by AMs and cDCs. Resembling the response in the absence of AMs, the failure in antiviral response by AMs and cDCs led to massive production of IFN-α from pDCs. Intranasal local infection of SeV Cm, however, induced IFN-α production from AMs, but not from pDCs. Thus, if SeV fails to subvert the host antiviral response due to its deficiency of C proteins, AMs will exert an effective antiviral response against SeV to control viral dissemination.

From these observations, we propose that three different IPCs in the lung, i.e. AMs, cDCs, and pDCs, are activated sequentially, but not simultaneously, for mounting antiviral immune responses. AMs act as the first-line sensor of invading viruses, and produce IFN-α at the site of infection. cDCs also initially produce IFN-α against viral infection, and have an additional role in producing IFNs in regional LNs. In contrast, pDCs are not activated until the initial defense line is broken by the viruses. It is of note that pDCs utilize the TLR system for type I IFN production, which is different from AM and cDC usage of the RLH system. Given that several virulent RNA viruses, such as SeV and influenza virus, suppress the RLH-mediated signaling pathway, type I IFN signaling pathway, or both (Kato et al., 2007; Pichlmair et al., 2006), it is tempting

to speculate that hosts have evolved two different type I IFN production systems to make it more difficult for viruses to escape the antiviral response.

This study showed that the *Ifna6*$^{gfp/+}$ mice are a quite useful tool for identifying IPCs in response to viral infection. Although we used respiratory virus infection as a model of local viral infection, as yet uncharacterized IPCs can be activated in other organs and mucosal tissues, such as intestine. Thus, this mouse model will be useful in identifing IPCs in different tissues in relation to various viral infections. Recent expansion in IFN biology has also revealed that type I IFNs are not only involved in antiviral responses, but also in responses to bacteria and autoimmune diseases (Banchereau and Pascual, 2006). For instance, overproduction of type I IFNs is reported in some autoimmune diseases, such as systemic lupus erythematosus, although the identity or identities of the type I IFN-producing cells are not clear in mouse models of the autoimmune disease. Therefore, we believe that this mouse model will benefit research in the IFN field by providing a vehicle for in vivo insights.

EXPERIMENTAL PROCEDURES

Generation of *Ifna6*^{gfp} Knockin Mice

The *Ifna6* gene and its flanking region were isolated from genomic DNA extracts of ES cells (clone GSI-I) by PCR. The targeting vector was constructed by replacing a 1.0 kb fragment encoding the entire *Ifna6* open reading frame with a neomycin-resistance gene cassette (*neo*) and a fragment encoding EGFP (*gfp*) from pEGFP-1 (Clontech). A herpes simplex virus thymidine kinase driven by PGK promoter (*HSV-Tk*) was inserted into the genomic fragment for negative selection. After the targeting vector was transfected into ES cells, G418 and gancyclovir doubly resistant colonies were selected and screened by PCR and Southern blotting. A plasmid that contains a gene encoding Cre recombinase was transfected into the clone and G418-sensitive colonies were selected. Clones in which excision of the *neo* gene took place were screened by Southern blotting. These clones were microinjected into C57BL/6 female mice, and heterozygous *Ifna6*$^{gfp/+}$ F1 progenies were backcrossed five times to C57BL/6 before analysis.

Mice

Mice deficient in *Myd88* and *Ips-1* have been described previously (Adachi et al., 1998; Kumar et al., 2006). All mice were bred and maintained in a specific pathogen-free facility of the Research Institute for Microbial Diseases, Osaka University, in accordance with the specifications of the Association for Assessment and Accreditation of Laboratory Animal Care. Mouse protocols were approved by Osaka University Animal Care and Use Committee.

Reagents and Viruses

All fluorochrome-conjugated and biotin-conjugated antibodies were purchased from BD PharMingen unless otherwise indicated. Flt3L was purchased from Peprotec. When administered intravenously, 5 μg of CpG-ODN D35 (Uematsu et al., 2005) was complexed to 30 μl of DOTAP transfection reagent (Boeringer-Manheim) at the final concentration of 25 μg/ml, and the conjugate was administered. R-848 has also been described (Hemmi et al., 2002), and 100 nmol of R-848 was administered intravenously. Poly (I:C) was purchased from Amersham, and 100 μg of poly (I:C) was intravenously administered. NDV and VSV-NCP were a kind gift from Dr. T. Abe and Dr. Y. Matsuura (Research Institute for Microbial Diseases, Osaka University). NDV suspended in chick allantoic fluid was administered both intravenously and intranasally at a titer of 1 × 10^7 plaque forming unit (pfu) after anesthesia. Allantoic fluid does not induce IFN-α either in vitro or in vivo by itself (data not shown). VSV-NCP was administered intravenously at a titer of 1 × 10^6 pfu. Wild-type SeV and SeV Cm were kindly provided by Dr. A. Kato (National Institute for Infectious Diseases, Japan) and administered both intravenously and intranasally at a titer of 1 × 10^7 pfu. The IFN-α ELISA kit was obtained from PBL.

Isolation of Cells from Tissues

Isolation of lung cells was performed as essentially described with some modifications (de Heer et al., 2004). Briefly, mice were sacrificed and perfused with PBS containing 10 mM EDTA from the right ventricle. Lung lobes were isolated and collagenase buffer (150 units/ml of collagenase [purchased from Wako Chemicals], 10 μg/ml of DNaseI [from Sigma], and 5% of FCS in RPMI1640 medium) was injected into the lobes using a 27G needle. The lobes were then shredded into small pieces and incubated at 37°C for 45 min. During the last 5 min, EDTA was added at 10 mM. Any remaining small pieces were dispersed by passage in and out through a 20G needle, and the suspension was passed through nylon mesh to remove debris. A single-cell suspension was prepared after RBC lysis. Cells from LNs (both inguinal and mediastinal) and liver were isolated essentially in the same manner as lung cells were.

Flow-Cytometric Analysis and Sorting

Intracellular staining of IFN-α was performed as described (Kato et al., 2005). For sorting pDCs, cDCs, and macrophages from spleen, $CD19^+$ cells and $Thy1.2^+$ cells in splenocytes were depleted by a magnetic bead sorting system using magnetic bead-conjugated anti-CD19 and anti-Thy1.2 antibodies (Miltenyi Biotech). The cells of the depleted fraction were stained with PerCP-conjugated anti-B220, APC-conjugated anti-CD11c, and FITC-conjugated anti-Mac-1 antibodies. Gates were set as in Figure 2A. For sorting AMs, a single-cell suspension of lung cells was stained with APC-conjugated anti-CD11c, FITC-conjugated anti-CD2, and PE-conjugated anti-Mac-1 antibodies. $CD11c^{hi}CD2^{hi}Mac\text{-}1^-$ cells were sorted as AMs. Stained cells were sorted using a FACSArea (BD Bioscience). Sorted cells had more than 95% purity.

Immunofluorescence Staining

Isolated tissues were embedded into OCT compound (Sakura Finetechnical) and subjected to rapid cooling in *n*-hexane cooled in liquid nitrogen and stored at −80°C until further analysis. Five-micrometer thick cryosections were fixed in acetone at −30°C for 20 min, air-dried, and rehydrated in PBS and PBS containing 0.05% Tween 20 (PBST) for 1 min each before staining. Sections were incubated in 2% BSA in PBST for 30 min at room temperature. If required, streptavidin-biotin blocking was also performed using a streptavidin-biotin blocking kit (Vector laboratories). After blocking, sections were stained with anti-GFP rabbit polyclonal antibody (SantaCruz) and anti-MAdCAM-1 rat monoclonal antibody (clone MECA75). Alexa 488-conjugated anti-rabbit IgG (Invitrogen) and biotinylated anti-rat IgG (Jackson Immunoresearch) were then applied as secondary antibodies. Finally, sections were stained with Alexa 594-conjugated streptavidin (Invitrogen). The resulting stained specimens were mounted by VectaShield Mounting Medium Hard (Vector Laboratories) and observed under an Olympus IX81 microscope (Olympus). Obtained images were processed using Metamorph software.

RNA Isolation; Q-PCR

Total RNA was isolated using TRIzol (Invitrogen) according to the manufacturer's instructions. One microgram of RNA was reverse transcribed using ReverTraAce (Toyobo) following the manufacturer's protocol. For sorting cells, total RNA was first purified using an RNA isolation and purification Mini Kit (QIAGEN), and 10 ng of obtained purified RNA was reverse transcribed using an Ovation Biotin System (Nugen) according to manufacturer's instructions. The resulting cDNA was subjected to Q-PCR as described (Matsui et al., 2006). Probes were purchased from Applied Biosystems. The probe for

a gene encoding NDV nucleocapsid protein has been described (Matsui et al., 2006).

Depletion of AMs with Cl_2MBP-Liposome

The preparation of liposomes was performed as described (Thepen et al., 1989) with some modifications. Briefly, cholesterol (CL, purchased from Sigma) and L-α-phosphatidylcholine (from yolk egg, Type XVI-E, Sigma) were dissolved in chloroform at concentrations of 8 and 100 mg/ml, respectively. One milliliter of CL solution was mixed with eighty-six microliters of PC solution in a two-milliliter tube. The chloroform in the mixture was evaporated in a centrifuge evaporator. Either 1 ml of PBS or Cl_2MBP (from Sigma) in PBS at a concentration of 0.25 g/ml was added into the tube and mixed well by mild vortexing for 30 min. The mixture was incubated at room temperature for 2 hr. It was then sonicated for 3 min in a waterbath sonicator and incubated for an additional 2 hr. The resulting liposomes were washed by PBS and resuspended in 200 μl of PBS. To deplete AMs in vivo, 50 μl of Cl_2MBP-liposome was administered intranasally. Twenty-four hours later, mice were subjected to further analysis.

Supplemental Data

The Supplemental Data, which consists of seven additional figures, can be found online at http://www.immunity.com/cgi/content/full/27/2/240/DC1/.

ACKNOWLEDGMENTS

We thank all colleagues in our laboratory; A. Kato, T. Abe, Y. Matsuura, T. Shioda, and E. Nakayama for providing viruses; K. Nakamura for cell sorting; P.Y. Lee for critical reading of the manuscript; M. Hashimoto for secretarial assistance; and Y. Fujiwara, M. Shiokawa, and N. Kitagaki for technical assistance.

This work was supported in part by grants from the Ministry of Education, Culture, Sports, Science, and Technology in Japan; the 21st Century Center of Excellence Program of Japan; and NIH (AI070167). The authors declare that they have no competing financial interests.

Received: March 16, 2007
Revised: May 22, 2007
Accepted: July 3, 2007
Published online: August 23, 2007

REFERENCES

Adachi, O., Kawai, T., Takeda, K., Matsumoto, M., Tsutsui, H., Sakagami, M., Nakanishi, K., and Akira, S. (1998). Targeted disruption of the MyD88 gene results in loss of IL-1- and IL-18-mediated function. Immunity *9*, 143–150.

Akira, S., Uematsu, S., and Takeuchi, O. (2006). Pathogen recognition and innate immunity. Cell *124*, 783–801.

Asselin-Paturel, C., Boonstra, A., Dalod, M., Durand, I., Yessaad, N., Dezutter-Dambuyant, C., Vicari, A., O'Garra, A., Biron, C., Briere, F., and Trinchieri, G. (2001). Mouse type I IFN-producing cells are immature APCs with plasmacytoid morphology. Nat. Immunol. *2*, 1144–1150.

Asselin-Paturel, C., Brizard, G., Chemin, K., Boonstra, A., O'Garra, A., Vicari, A., and Trinchieri, G. (2005). Type I interferon dependence of plasmacytoid dendritic cell activation and migration. J. Exp. Med. *201*, 1157–1167.

Banchereau, J., and Pascual, V. (2006). Type I interferon in systemic lupus erythematosus and other autoimmune diseases. Immunity *25*, 383–392.

Barchet, W., Cella, M., Odermatt, B., Asselin-Paturel, C., Colonna, M., and Kalinke, U. (2002). Virus-induced interferon alpha production by a dendritic cell subset in the absence of feedback signaling in vivo. J. Exp. Med. *195*, 507–516.

Bjorck, P. (2001). Isolation and characterization of plasmacytoid dendritic cells from Flt3 ligand and granulocyte-macrophage colony-stimulating factor-treated mice. Blood *98*, 3520–3526.

Cella, M., Jarrossay, D., Facchetti, F., Alebardi, O., Nakajima, H., Lanzavecchia, A., and Colonna, M. (1999). Plasmacytoid monocytes migrate to inflamed lymph nodes and produce large amounts of type I interferon. Nat. Med. *5*, 919–923.

Chan, C.W., Crafton, E., Fan, H.N., Flook, J., Yoshimura, K., Skarica, M., Brockstedt, D., Dubensky, T.W., Stins, M.F., Lanier, L.L., et al. (2006). Interferon-producing killer dendritic cells provide a link between innate and adaptive immunity. Nat. Med. *12*, 207–213.

Dalod, M., Salazar-Mather, T.P., Malmgaard, L., Lewis, C., Asselin-Paturel, C., Briere, F., Trinchieri, G., and Biron, C.A. (2002). Interferon alpha/beta and interleukin 12 responses to viral infections: pathways regulating dendritic cell cytokine expression in vivo. J. Exp. Med. *195*, 517–528.

de Heer, H.J., Hammad, H., Soullie, T., Hijdra, D., Vos, N., Willart, M.A., Hoogsteden, H.C., and Lambrecht, B.N. (2004). Essential role of lung plasmacytoid dendritic cells in preventing asthmatic reactions to harmless inhaled antigen. J. Exp. Med. *200*, 89–98.

Diebold, S.S., Montoya, M., Unger, H., Alexopoulou, L., Roy, P., Haswell, L.E., Al-Shamkhani, A., Flavell, R., Borrow, P., and Reis e Sousa, C. (2003). Viral infection switches non-plasmacytoid dendritic cells into high interferon producers. Nature *424*, 324–328.

Hashimoto, Y., Moki, T., Takizawa, T., Shiratsuchi, A., and Nakanishi, Y. (2007). Evidence for phagocytosis of influenza virus-infected, apoptotic cells by neutrophils and macrophages in mice. J. Immunol. *178*, 2448–2457.

Hemmi, H., Kaisho, T., Takeuchi, O., Sato, S., Sanjo, H., Hoshino, K., Horiuchi, T., Tomizawa, H., Takeda, K., and Akira, S. (2002). Small anti-viral compounds activate immune cells via the TLR7 MyD88-dependent signaling pathway. Nat. Immunol. *3*, 196–200.

Honda, K., Yanai, H., Mizutani, T., Negishi, H., Shimada, N., Suzuki, N., Ohba, Y., Takaoka, A., Yeh, W.C., and Taniguchi, T. (2004). Role of a transductional-transcriptional processor complex involving MyD88 and IRF-7 in Toll-like receptor signaling. Proc. Natl. Acad. Sci. USA *101*, 15416–15421.

Honda, K., Yanai, H., Negishi, H., Asagiri, M., Sato, M., Mizutani, T., Shimada, N., Ohba, Y., Takaoka, A., Yoshida, N., and Taniguchi, T. (2005). IRF-7 is the master regulator of type-I interferon-dependent immune responses. Nature *434*, 772–777.

Honda, K., Takaoka, A., and Taniguchi, T. (2006). Type I interferon [corrected] gene induction by the interferon regulatory factor family of transcription factors. Immunity *25*, 349–360.

Hornung, V., Ellegast, J., Kim, S., Brzozka, K., Jung, A., Kato, H., Poeck, H:, Akira, S., Conzelmann, K.K., Schlee, M., et al. (2006). 5′-Triphosphate RNA is the ligand for RIG-I. Science *314*, 994–997.

Hoshino, K., Sugiyama, T., Matsumoto, M., Tanaka, T., Saito, M., Hemmi, H., Ohara, O., Akira, S., and Kaisho, T. (2006). IkappaB kinase-alpha is critical for interferon-alpha production induced by Toll-like receptors 7 and 9. Nature *440*, 949–953.

Kato, A., Kiyotani, K., Kubota, T., Yoshida, T., Tashiro, M., and Nagai, Y. (2007). Importance of Anti-Interferon Capacity of the Sendai Virus C Protein for Pathogenicity in Mice. J Virol. *81*, 3264–3271.

Kato, H., Sato, S., Yoneyama, M., Yamamoto, M., Uematsu, S., Matsui, K., Tsujimura, T., Takeda, K., Fujita, T., Takeuchi, O., and Akira, S. (2005). Cell type-specific involvement of RIG-I in antiviral response. Immunity *23*, 19–28.

Kato, H., Takeuchi, O., Sato, S., Yoneyama, M., Yamamoto, M., Matsui, K., Uematsu, S., Jung, A., Kawai, T., Ishii, K.J., et al. (2006). Differential roles of MDA5 and RIG-I helicases in the recognition of RNA viruses. Nature *441*, 101–105.

Kawai, T., and Akira, S. (2006). Innate immune recognition of viral infection. Nat. Immunol. *7*, 131–137.

Kawai, T., Sato, S., Ishii, K.J., Coban, C., Hemmi, H., Yamamoto, M., Terai, K., Matsuda, M., Inoue, J., Uematsu, S., et al. (2004). Interferon-alpha induction through Toll-like receptors involves a direct interaction of IRF7 with MyD88 and TRAF6. Nat. Immunol. *5*, 1061–1068.

Kawai, T., Takahashi, K., Sato, S., Coban, C., Kumar, H., Kato, H., Ishii, K.J., Takeuchi, O., and Akira, S. (2005). IPS-1, an adaptor triggering RIG-I- and Mda5-mediated type I interferon induction. Nat. Immunol. *6*, 981–988.

Kumar, H., Kawai, T., Kato, H., Sato, S., Takahashi, K., Coban, C., Yamamoto, M., Uematsu, S., Ishii, K.J., Takeuchi, O., and Akira, S. (2006). Essential role of IPS-1 in innate immune responses against RNA viruses. J. Exp. Med. *203*, 1795–1803.

Louten, J., van Rooijen, N., and Biron, C.A. (2006). Type 1 IFN deficiency in the absence of normal splenic architecture during lymphocytic choriomeningitis virus infection. J. Immunol. *177*, 3266–3272.

Matsui, K., Kumagai, Y., Kato, H., Sato, S., Kawagoe, T., Uematsu, S., Takeuchi, O., and Akira, S. (2006). Cutting edge: Role of TANK-binding kinase 1 and inducible IkappaB kinase in IFN responses against viruses in innate immune cells. J. Immunol. *177*, 5785–5789.

Meylan, E., Curran, J., Hofmann, K., Moradpour, D., Binder, M., Bartenschlager, R., and Tschopp, J. (2005). Cardif is an adaptor protein in the RIG-I antiviral pathway and is targeted by hepatitis C virus. Nature *437*, 1167–1172.

Nakano, H., Yanagita, M., and Gunn, M.D. (2001). CD11c(+)B220(+)Gr-1(+) cells in mouse lymph nodes and spleen display characteristics of plasmacytoid dendritic cells. J. Exp. Med. *194*, 1171–1178.

Peters-Golden, M. (2004). The alveolar macrophage: the forgotten cell in asthma. Am. J. Respir. Cell Mol. Biol. *31*, 3–7.

Pichlmair, A., Schulz, O., Tan, C.P., Naslund, T.I., Liljestrom, P., Weber, F., and Reis e Sousa, C. (2006). RIG-I-mediated antiviral responses to single-stranded RNA bearing 5′-phosphates. Science *314*, 997–1001.

Prakash, A., Smith, E., Lee, C.K., and Levy, D.E. (2005). Tissue-specific positive feedback requirements for production of type I interferon following virus infection. J. Biol. Chem. *280*, 18651–18657.

Seth, R.B., Sun, L., Ea, C.K., and Chen, Z.J. (2005). Identification and characterization of MAVS, a mitochondrial antiviral signaling protein that activates NF-kappaB and IRF 3. Cell *122*, 669–682.

Siegal, F.P., Kadowaki, N., Shodell, M., Fitzgerald-Bocarsly, P.A., Shah, K., Ho, S., Antonenko, S., and Liu, Y.J. (1999). The nature of the principal type 1 interferon-producing cells in human blood. Science *284*, 1835–1837.

Stetson, D.B., and Medzhitov, R. (2006). Type I interferons in host defense. Immunity *25*, 373–381.

Sun, Q., Sun, L., Liu, H.H., Chen, X., Seth, R.B., Forman, J., and Chen, Z.J. (2006). The specific and essential role of MAVS in antiviral innate immune responses. Immunity *24*, 633–642.

Taieb, J., Chaput, N., Menard, C., Apetoh, L., Ullrich, E., Bonmort, M., Pequignot, M., Casares, N., Terme, M., Flament, C., et al. (2006). A novel dendritic cell subset involved in tumor immunosurveillance. Nat. Med. *12*, 214–219.

Thepen, T., Van Rooijen, N., and Kraal, G. (1989). Alveolar macrophage elimination in vivo is associated with an increase in pulmonary immune response in mice. J. Exp. Med. *170*, 499–509.

Uematsu, S., Sato, S., Yamamoto, M., Hirotani, T., Kato, H., Takeshita, F., Matsuda, M., Coban, C., Ishii, K.J., Kawai, T., et al. (2005). Interleukin-1 receptor-associated kinase-1 plays an essential role for Toll-like receptor (TLR)7- and TLR9-mediated interferon-{alpha} induction. J. Exp. Med. *201*, 915–923.

Vremec, D., O'Keeffe, M., Hochrein, H., Fuchsberger, M., Caminschi, I., Lahoud, M., and Shortman, K. (2007). Production of interferons by dendritic cells, plasmacytoid cells, natural killer cells, and interferon-producing killer dendritic cells. Blood *109*, 1165–1173.

Woodland, D.L., Hogan, R.J., and Zhong, W. (2001). Cellular immunity and memory to respiratory virus infections. Immunol. Res. *24*, 53–67.

Xu, L.G., Wang, Y.Y., Han, K.J., Li, L.Y., Zhai, Z., and Shu, H.B. (2005). VISA is an adapter protein required for virus-triggered IFN-beta signaling. Mol. Cell *19*, 727–740.

Yoneyama, M., Kikuchi, M., Natsukawa, T., Shinobu, N., Imaizumi, T., Miyagishi, M., Taira, K., Akira, S., and Fujita, T. (2004). The RNA helicase RIG-I has an essential function in double-stranded RNA-induced innate antiviral responses. Nat. Immunol. *5*, 730–737.

Yoneyama, H., Matsuno, K., Toda, E., Nishiwaki, T., Matsuo, N., Nakano, A., Narumi, S., Lu, B., Gerard, C., Ishikawa, S., and Matsushima, K. (2005). Plasmacytoid DCs help lymph node DCs to induce anti-HSV CTLs. J. Exp. Med. *202*, 425–435.

Essential role of IRAK-4 protein and its kinase activity in Toll-like receptor–mediated immune responses but not in TCR signaling

Tatsukata Kawagoe,[1,2] Shintaro Sato,[2] Andreas Jung,[1] Masahiro Yamamoto,[1] Kosuke Matsui,[1,2] Hiroki Kato,[1] Satoshi Uematsu,[1] Osamu Takeuchi,[1,2] and Shizuo Akira[1,2]

[1]Department of Host Defense, Research Institute for Microbial Diseases, Osaka University, Suita, Osaka 565-0871, Japan
[2]Exploratory Research for Advanced Technology, Japan Science and Technology Agency, Suita, Osaka 565-0871, Japan

Interleukin-1 receptor–associated kinase 4 (IRAK-4) was reported to be essential for the Toll-like receptor (TLR)– and T cell receptor (TCR)–mediated signaling leading to the activation of nuclear factor κB (NF-κB). However, the importance of kinase activity of IRAK family members is unclear. In this study, we investigated the functional role of IRAK-4 activity in vivo by generating mice carrying a knockin mutation (KK213AA) that abrogates its kinase activity. *IRAK-4*$^{KN/KN}$ mice were highly resistant to TLR-induced shock response. The cytokine production in response to TLR ligands was severely impaired in *IRAK-4*$^{KN/KN}$ as well as *IRAK-4*$^{-/-}$ macrophages. The IRAK-4 activity was essential for the activation of signaling pathways leading to mitogen-activated protein kinases. TLR-induced IRAK-4/IRAK-1–dependent and –independent pathways were involved in early induction of NF-κB–regulated genes in response to TLR ligands such as tumor necrosis factor α and IκBζ. In contrast to a previous paper (Suzuki, N., S. Suzuki, D.G. Millar, M. Unno, H. Hara, T. Calzascia, S. Yamasaki, T. Yokosuka, N.J. Chen, A.R. Elford, et al. 2006. *Science.* 311:1927–1932), the TCR signaling was not impaired in *IRAK-4*$^{-/-}$ and *IRAK-4*$^{KN/KN}$ mice. Thus, the kinase activity of IRAK-4 is essential for the regulation of TLR-mediated innate immune responses.

CORRESPONDENCE
Shizuo Akira:
sakira@biken.osaka-u.ac.jp

Abbreviations used: Ab, antibody; COX-2, cyclooxygenase-2; EMSA, electrophoretic mobility shift assay; ERK, extracellular signal-regulated kinase; ES, embryonic stem; IKK-γ, IκB kinase γ; IL-1R, IL-1 receptor; IRAK, IL-1R–associated kinase; JNK, c-Jun N-terminal kinase; LCMV, lymphocytic choriomeningitis virus; MALP-2, macrophage-activating lipopeptide-2; MAP, mitogen-activated protein; MEF, mouse embryonic fibroblast; mRNA, messenger RNA; pDC, plasmacytoid DC; TIR, Toll/IL-1R; TLR, Toll-like receptor; TRAF6, TNF receptor–associated factor 6.

The innate immune system senses pathogen-specific molecular patterns via pattern recognition receptors, such as Toll-like receptors (TLRs; references 1–3). 12 TLR family members have been identified in mammals, and the pathogen-specific molecular patterns recognized by these TLRs have been mostly identified. The cytoplasmic portion of TLRs, called TIR (Toll/IL-1 receptor [IL-1R]) domain, resembles that of IL-1R family members, and these two receptor families in part share intracellular signaling machineries. Stimulation with TLR ligands or IL-1 family cytokines recruits a TIR domain–containing adaptor, MyD88, to the receptors. IL-1R–associated kinases (IRAKs) are recruited to MyD88 through a homophilic interaction of the death domains and associate with TNF receptor–associated factor 6 (TRAF6), which acts as an ubiquitin protein ligase. TRAF6 catalyzes the formation of a K63-linked polyubiquitin chain on TRAF6 itself and on IκB kinase γ (IKK-γ)/NF-κB essential modulator. TGF-β–activated kinase 1 is also recruited to TRAF6 and then phosphorylates IKK-β and mitogen-activated protein (MAP) kinase kinase 6. Phosphorylation of IκB by the IKK complex leads to its degradation, and freed NF-κB translocates into the nucleus, resulting in induction of genes involved in inflammatory responses as well as increase in the surface expression of costimulatory molecules on innate immune cells. The activation of MAP kinase cascade is responsible for AP-1–induced gene expression. In addition to the MyD88-dependent signaling pathway, the TLR4 signaling also activates a MyD88-independent signaling cascade via another TIR domain–containing adaptor protein inducing IFN-β, TRIF (4). It triggers the signaling cascade leading to the production of type I IFNs

The online version of this article contains supplemental material.

via IKK-related kinases, TANK-binding kinase 1 (TBK1) and IKK-*i*. The TLR3 signaling also entirely relies on TRIF to activate NF-κB and IFN-regulatory factors.

The IRAK family is comprised of four members and is characterized by the presence of an N-terminal death domain and a serine/threonine kinase domain (5). IRAK-1 was initially identified as a kinase that is coprecipitated with IL-1R in response to IL-1 stimulation (6). IRAK-1 associates with MyD88 through a homophilic interaction of the death domains (7). Whereas IRAK-1 has a nonredundant role in the production of type I IFNs in response to TLR9 ligands in plasmacytoid DCs (pDCs; reference 8), IRAK1-deficient (*IRAK-1*$^{-/-}$) macrophages show modest impairment in IL-1R– and TLR-mediated proinflammatory cytokine production (9, 10). IRAK-2 is suggested to be involved in the signaling via TIRAP/Mal, an adaptor protein responsible for TLR2 and TLR4 responses (11). In contrast, IRAK-M was identified as the negative regulator of the TLR/IL-1R signaling (12). The fourth member of IRAK family members, IRAK-4, has been discovered by a database search (13). Generation of *IRAK-4*$^{-/-}$ mice revealed its essential role in IL-1R/TLR–mediated responses (14, 15). Furthermore, the poor defenses against bacterial infection were observed in patients having autosomal recessive amorphic mutations in IRAK-4 (16, 17). It was suggested that IRAK-4 can directly phosphorylate IRAK-1 for the signaling. Recently, IRAK-4 has been reported to be a requisite for TCR-induced NF-κB activation by associating with ZAP-70 (18).

Although IRAK family members are involved in TLR/IL-1R signaling, the role of their kinase activity is still controversial. Among IRAK family members, IRAK-1 and -4 were shown to possess intrinsic kinase activity (13, 19). Nevertheless, it has been shown that IRAK-1 kinase activity is dispensable for its ability to activate NF-κB (20). IRAK-1 could act as a scaffold protein recruiting MyD88 and TRAF6 for the signaling (13). Second, a critical aspartate residue in the catalytic domain has changed to an asparagine or a serine in IRAK-2 or -M, and their kinase domains have been shown to be inactive (21). Regarding the requirement of IRAK-4 activity for the IL-1R signaling, two controversial observations have been reported to date (22, 23). One paper showed that the reconstitution with the kinase-inactive mutant IRAK-4 fully restored IL-1 responsiveness (22), whereas the other showed that the same reconstitution was capable of restoring only a partial cytokine response to IL-1β (23). Therefore, the requirement of kinase activity in IRAK family members has not been well understood.

In the present study, we generated mice carrying a knockin mutation that abrogated IRAK-4 activity. For the assessment of the roles of kinase activity, we also generated *IRAK-4*$^{-/-}$ mice. The analysis of these mice revealed that the kinase activity of IRAK-4 is essential for the physiological function of IRAK-4, and the TLR-mediated proinflammatory responses are severely impaired in these mice. Nevertheless, we did not observe any defects in the T cell responses in either *IRAK-4*$^{-/-}$ or *IRAK-4*$^{KN/KN}$ mice. This study demonstrates

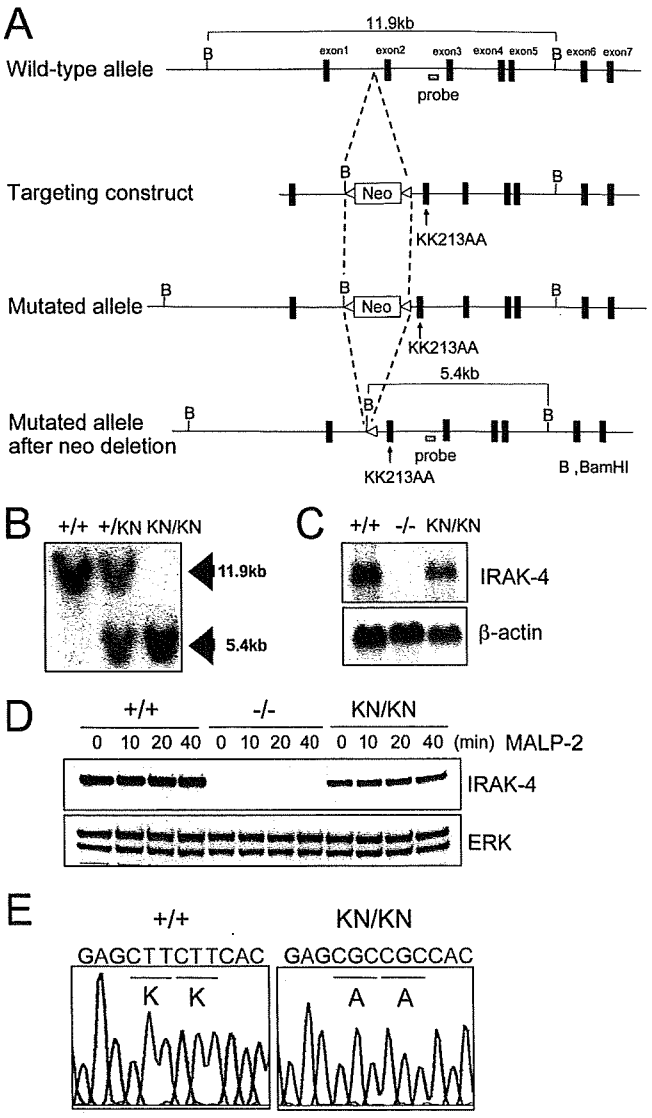

Figure 1. Generation of *IRAK-4*$^{KN/KN}$ mice. (A) Schematic representation of IRAK-4 (KK213AA) knockin allele. The targeting vector contains point mutations in exon 2 that change lysines at position 213 and 214 to alanine (KK213AA). (B) Southern blot analysis of offspring from the heterozygote intercrosses. Genomic DNA was extracted from mouse tails, digested with BamHI, separated by electrophoresis, and hybridized with the radiolabeled probe indicated in A. (C) Nothern blot analysis of the expression of IRAK-4 mRNA. Total RNA from wild-type, *IRAK-4*$^{-/-}$, and *IRAK-4*$^{KN/KN}$ peritoneal macrophages were extracted and subjected to the Northern blot analysis for the expression of IRAK-4 mRNA. The same membrane was rehybridized with a β-actin probe. (D) Immunoblot analysis for the expression of IRAK-4 protein expression in wild-type (+/+), *IRAK-4*$^{-/-}$ (−/−), and *IRAK-4*$^{KN/KN}$ (KN/KN) macrophages. Cell lysates from peritoneal macrophages stimulated with 10 ng/ml MALP-2 for the indicated times were immunoblotted with Ab to IRAK-4. Probing for ERK1/2 was used to ensure equal loading. (E) PCR amplification products from wild-type (+/+) and *IRAK-4*$^{KN/KN}$ (KN/KN) macrophages were subcloned and sequenced to demonstrate the presence of the KK213AA mutation; representative traces are shown.

that IRAK-4 functions as an actual kinase for relaying the TLR signaling.

RESULTS

Generation of *IRAK-4*$^{KN/KN}$ and *IRAK-4*$^{-/-}$ mice

It has been shown that a mutation in ATP binding pocket (K239S) of IRAK-1 abrogated its kinase activity. Nevertheless, overexpression of this mutant IRAK-1 still efficiently induced NF-κB activation. Corresponding mutations in IRAK-4 (KK213AA) was capable of inducing activation of NF-κB in response to IL-1β stimulation. These results suggested that IRAK family members function as adaptor molecules for the signaling, and the IRAK kinase activity was dispensable for their function. To identify the role of IRAK-4 activity in TLR signaling, we inserted a mutation (KK213AA) of IRAK-4. To replace serines 213 and 214 of IRAK-4 with alanines, a loxP-flanked Neo cassette was inserted. Serine to alanine substitutions were introduced by site-directed mutagenesis (Fig. 1 A). A targeting vector containing these mutations were electroporated into embryonic stem (ES) cells, clones with homologous recombination at the IRAK-4 locus were obtained, and IRAK-4–mutated mice were generated. The mice were crossed with CAG-Cre transgenic mice to excise the neo resistant gene. Homologous recombination of IRAK-4 locus was confirmed by Southern blotting, and the sequencing analysis revealed that the mutations were correctly introduced (Fig. 1, B and E). The Northern blot and immunoblot analysis showed that IRAK-4 messenger RNA (mRNA) and protein were expressed in wild-type and *IRAK-4*$^{KN/KN}$ macrophages, although the expression of IRAK-4 protein was slightly reduced in *IRAK-4*$^{KN/KN}$ macrophages (Fig. 1, C and D).

We also generated *IRAK-4*$^{-/-}$ mice by homologous recombination to compare the importance of kinase activity of IRAK-4 (Fig. S1, A and B, available at http://www.jem.org/cgi/content/full/jem.20061523/DC1). For generation of *IRAK-4*$^{-/-}$ mice, we targeted exon 2 of mouse IRAK-4 gene with the neo cassette in ES cells and established *IRAK-4*$^{-/-}$ mice. Absence of IRAK-4 protein in *IRAK-4*$^{-/-}$ macrophages was confirmed by Northern blotting and immunoblotting (Fig. 1, C and D).

In vitro kinase assay revealed that IRAK-4 autophosphorylation was induced in wild-type macrophages in response to TLR2 stimulation (Fig. 2 A). In contrast, the autophosphorylation of IRAK-4 was not observed either in *IRAK-4*$^{KN/KN}$ or *IRAK-4*$^{-/-}$ cells. To further investigate whether the mutant IRAK-4 can phosphorylate IRAK-1, we isolated IRAK-4 cDNA from wild-type and *IRAK-4*$^{KN/KN}$ cells. The IRAK-4 proteins were expressed using the rabbit reticulocyte lysate system, and in vitro kinase assay was performed with mouse IRAK-1 protein (aa 301–500), which contains an activation loop, as a substrate. As shown in Fig. 2 B, the wild-type IRAK-4, but not IRAK-4 (KK213AA), phosphorylated IRAK-1. Immunoblot analysis revealed that the amounts of wild-type and IRAK-4 (KK213AA) expressed were not altered (Fig. 2 B).

We next examined whether IRAK-4 activity was required for the recruitment of IRAK-4 in the complex of

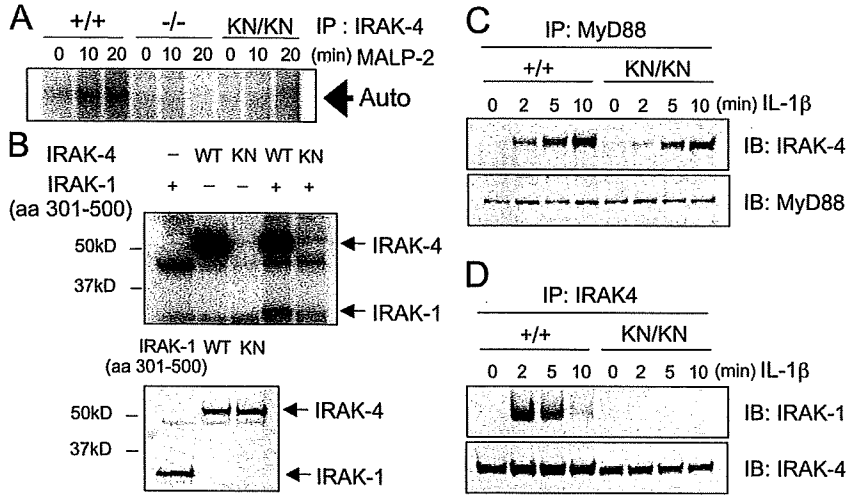

Figure 2. The kinase activity in *IRAK-4*$^{KN/KN}$ mice. (A) Peritoneal macrophages were stimulated with 10 ng/ml MALP-2 for 0, 10, and 20 min. The cell lysates were prepared and immunoprecipitated with anti-IRAK-4 Ab. The kinase activity of IRAK-4 was measured by in vitro kinase assay. The data shown are representative of three independent experiments. Auto, autophosphorylation. (B) IRAK-4 cDNA was obtained from total RNA of wild-type and *IRAK-4*$^{KN/KN}$ macrophages. Wild-type and KK213AA IRAK-4 proteins were expressed in the rabbit reticulocyte lysates, and in vitro kinase assay was performed in the presence of IRAK-1 (aa 301–500; top panel). The expression of wild-type and KK213AA IRAK-4 and IRAK-1 (aa 301–500) was determined by immunoblot analysis (bottom panel). (C) Interaction of MyD88 and IRAK-4. MEFs were stimulated with 10 ng/ml IL-1β for the indicated periods. The cell lysates were immunoprecipitaed with anti-MyD88, followed by immunoblot with anti-IRAK-4 and anti-MyD88. (D) IL-1β–induced coprecipitation of IRAK-1 and -4. The cell lysates prepared in C were immunoprecipitated with anti-IRAK-4, followed by immunoblot with anti-IRAK-1 and anti-IRAK-4.

MyD88 and IRAK-1 in response to IL-1R stimulation. When mouse embryonic fibroblasts (MEFs) were stimulated with IL-1β, IRAK-4 was coprecipitaited with MyD88 in both wild-type and *IRAK-4*$^{KN/KN}$ cells (Fig. 2 C). In contrast, interaction between IRAK-4 and -1 was not induced in *IRAK-4*$^{KN/KN}$ macrophages (Fig. 2 D). These results indicate that IRAK-4 activity is dispensable for the recruitment of IRAK-4 to MyD88, although the kinase activity is essential for the recruitment of IRAK-1 to -4.

The role of IRAK-4 activity in TLR-induced responses

We first examined the role of IRAK-4 activity in response to TLR ligand stimulation in vivo. After challenge with LPS or CpG-DNA together with D-galactosamine, wild-type mice succumbed to shock and died, whereas all *IRAK-4*$^{-/-}$ and *IRAK-4*$^{KN/KN}$ mice survived, indicating that the kinase activity of IRAK-4 is critical for the TLR-induced shock in vivo (Fig. 3, A and B). We examined cytokine production of macrophages possessing mutated IRAK-4 against TLR ligands, including macrophage-activating lipopeptide-2 (MALP-2; TLR6/TLR2), poly I:C (TLR3), LPS (TLR4), R-848 (TLR7), and CpG-DNA (TLR9). Thioglycollate-elicited peritoneal macrophages were stimulated with each TLR ligand and the production of proinflammatory cytokines was measured by ELISA. In accordance with a previous paper, production of IL-6, TNF-α, and IL-12p40 in response to these TLR ligands except poly I:C was severely impaired in *IRAK-4*$^{-/-}$ macrophages compared with wild-type cells (14). The production of IL-6, TNF-α, and IL-12p40 was also profoundly impaired in *IRAK-4*$^{KN/KN}$ cells, and the extent of reduction was similar to that of *IRAK-4*$^{-/-}$ cells (Fig. 3, C–E). In contrast, IL-6 and TNF-α production in response to poly I:C was not altered between wild-type, *IRAK-4*$^{-/-}$, and *IRAK-4*$^{KN/KN}$ macrophages. DCs from *IRAK-4*$^{KN/KN}$ mice also showed defective cytokine production in response to these TLR ligands (unpublished data). Thus, the IRAK-4 activity is important for evoking cytokine production in response to various TLR ligands, except for TLR3 ligand.

Not only proinflammatory cytokines but also type I IFNs are strongly induced in response to TLR7 and TLR9 stimulation in pDCs (8, 17, 24). It has been shown that IRAK-4 and -1 are essential for TLR9-induced type I IFN production in pDCs. To examine the role of IRAK-4 activity in type I IFN response, we generated pDCs by cultivating bone-marrow cells in the presence of Flt3 ligand. Whereas wild-type Flt3L-DCs produced IFN-α and IL-6 in response to A/D-type

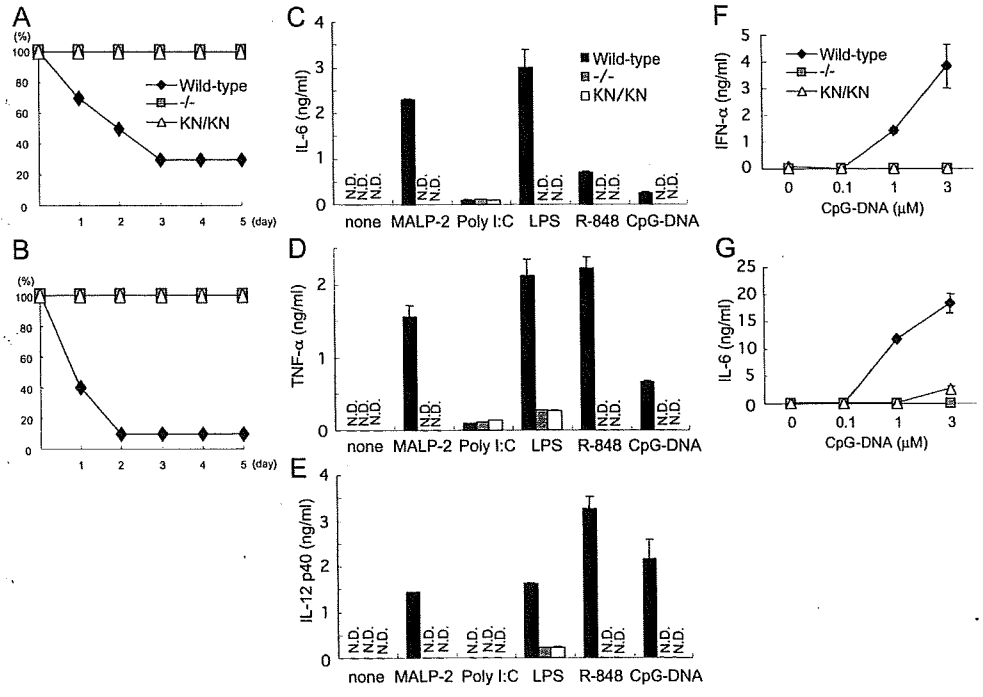

Figure 3. Essential role of IRAK-4 activity in TLR-mediated cytokine responses. (A and B) Age-matched wild-type ($n = 10$), *IRAK-4*$^{-/-}$ ($n = 5$), and *IRAK-4*$^{KN/KN}$ ($n = 5$) mice were challenged with 2 mg LPS (A) and 20 nmol CpG-DNA together with 20 mg D-galactosamine (B). The survival of mice was monitored for 5 d. (C–E) Thioglycollate-elicited peritoneal macrophages from wild-type, *IRAK-4*$^{-/-}$, and *IRAK-4*$^{KN/KN}$ mice were stimulated with MALP-2, poly I:C, LPS, R-848, and CpG-DNA for 24 h. For measuring IL-12 p40 concentration, macrophages were stimulated with the indicated TLR ligands in the presence of 30 ng/ml IFN-γ. Concentrations of IL-6 (C), TNF-α (D), and IL-12 p40 (E) in the culture supernatants were measured by ELISA. Data are shown as mean ± SD of triplicates. Similar results were obtained in three independent experiments. (F and G) Flt3L-DCs from wild-type, *IRAK-4*$^{-/-}$, and *IRAK-4*$^{KN/KN}$ mice were stimulated with the indicated concentrations of A/D type CpG-DNA. Production of IFN-α (D) and IL-6 (E) was measured by ELISA. Data are representative of three independent experiments. Indicated values are mean ± SD of triplicates.

CpG-DNA, cells from neither *IRAK-4*$^{-/-}$ nor *IRAK-4*$^{KN/KN}$ mice produced both IFN-α and IL-6 (Fig. 3, F and G).

Next we investigated the proliferation of B cells in response to these TLR ligands. When we stimulated purified B cells with MALP-2, poly I:C, LPS, R-848, and CpG-DNA, wild-type B cells proliferated in a dose-dependent manner (Fig. 4). In contrast, *IRAK-4*$^{-/-}$ as well as *IRAK-4*$^{KN/KN}$ B cells failed to proliferate in response to MALP-2, LPS, R-848, and CpG-DNA. Stimulation with poly I:C induced proliferation of B cells even in *IRAK-4*$^{-/-}$ and *IRAK-4*$^{KN/KN}$ mice, suggesting that TLR3 signals independent of IRAK-4 in B cells. The proliferative responses against anti-IgM, anti-CD40 antibodies (Abs) were not altered in wild-type, *IRAK-4*$^{-/-}$, and *IRAK-4*$^{KN/KN}$ splenocytes, indicating that the MyD88-dependent responses were specifically impaired in *IRAK-4*$^{-/-}$ or *IRAK-4*$^{KN/KN}$ cells. Collectively, the kinase activity of IRAK-4 is essential for the pleiotrophic effects in response to TLR stimulation.

Expression of TLR-mediated gene expression in IRAK-4 mutated mice

We examined whether the defects in cytokine response to TLR stimulation in IRAK-4 mutation were regulated in a gene expression level by Northern blot analysis. We chose TLR2 ligands as the stimulant because TLR2 signals only via the MyD88-dependent pathway. In response to MALP-2 stimulation, wild-type macrophages induced expression of IL-6, TNF-α, IκBζ, and cyclooxygenase-2 (COX-2) genes (Fig. 5 A). In contrast, *IRAK-4*$^{-/-}$ and *IRAK-4*$^{KN/KN}$ macrophages failed to express IL-6 and COX-2 in response to MALP-2 stimulation. However, TNF-α and IκBζ were expressed even in the absence of IRAK-4, albeit the expression was weaker than wild-type cells. Thus, the kinase activity of IRAK-4 is critical for regulating IRAK-4–mediated controlling of gene expression. Indeed, TNF bioassay revealed that a subtle amount of TNF activity was induced 1 and 2 h after MALP-2 stimulation in *IRAK-4*$^{-/-}$ and *IRAK-4*$^{KN/KN}$ macrophages, although the amount was much smaller than in wild-type cells (Fig. S2, available at http://www.jem.org/cgi/content/full/jem.20061523/DC1). Interestingly, MyD88$^{-/-}$ macrophages failed to induce any detectable amount of these genes in response to MALP-2 stimulation (Fig. 5 A). In addition, PAM_3CSK_4, a synthetic lipopeptide known to be recognized by TLR1/TLR2 heterodimer, also induces expression of TNF-α and IκBζ even in the absence of IRAK-4 (Fig. 5 B; reference 25). These results indicate that the early expression of TNF-α and IκBζ genes in response to TLR2 ligands is regulated in part in a IRAK-4–independent fashion, although IRAK-4 plays a major role in the expression of TLR2-inducible genes.

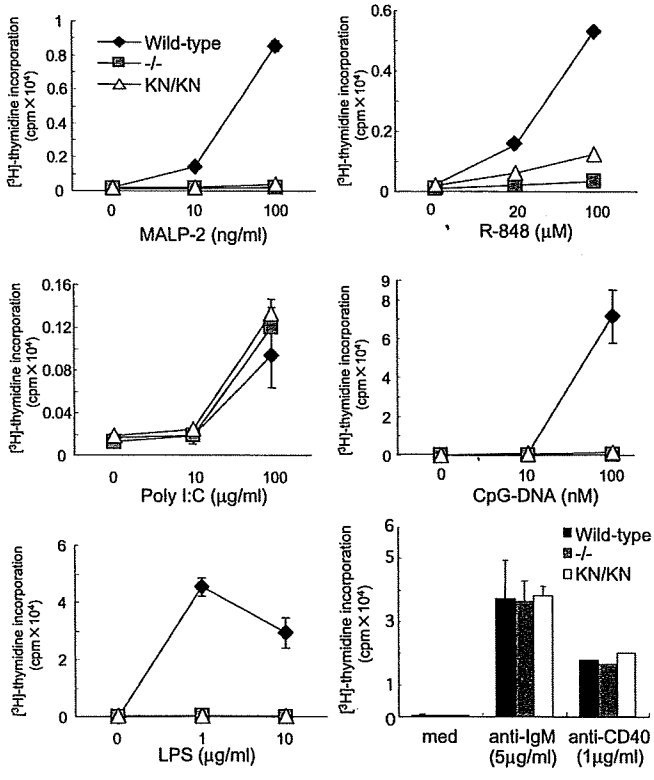

Figure 4. IRAK-4 activity is critical for TLR-mediated proliferation of splenocytes. Splenocytes were cultured with the indicated concentrations of MALP-2, poly I:C, LPS, R-848, CpG-DNA, anti-IgM, or anti-CD40 for 48 h. Samples were pulsed with 1 μCi [3H]thymidine for the last 16 h. [3H]thymidine incorporation was measured by a scintillation counter. Data are representative of three independent experiments. Indicated values are mean ± SD of triplicates.

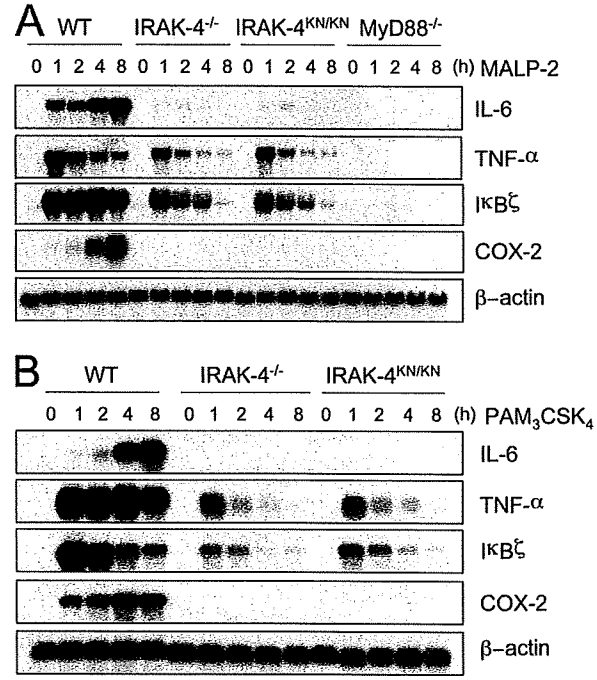

Figure 5. IRAK-4–independent induction of gene expression in TLR signaling. (A and B) Peritoneal macrophages were stimulated with 10 ng/ml MALP-2 (A) and 10 ng/ml PAM_3CSK_4 (B) for the indicated periods. Total RNA was extracted and subjected to Northern blot analysis for expression of IL-6, TNF-α, Iκ Bζ, and COX-2. The same membrane was rehybridized with a β-actin probe.

The role of IRAK-4 activity in the TLR-mediated signaling pathway

These observations prompted us to examine intracellular signaling pathways in response to TLR stimulation. It has been shown that IRAK-4 is recruited to IL-1R in response to ligand stimulation, where it phosphorylates and activates IRAK-1. It was also shown that IRAK-4 is essential for the initiation of IL-1R–mediated signaling pathways leading to the activation of NF-κB and MAP kinases in MEFs (14).

TLR2-mediated autophosphorylation of IRAK-1 was completely abrogated in *IRAK-4*$^{-/-}$ and *IRAK-4*$^{KN/KN}$ macrophages (Fig. 6 A). TLR/IL-1R stimulation induces not only phosphorylation but also degradation of IRAK-1. MALP-2 stimulation decreased the IRAK-1 expression in wild-type macrophages (Fig. 6 B). However, TLR2-mediated degradation of IRAK-1 was not observed in *IRAK-4*$^{-/-}$ and *IRAK-4*$^{KN/KN}$ macrophages. Thus, IRAK-4 activity is essential for IRAK-1 activation in response to TLR2 activation.

We examined the role of IRAK-4 activity in the activation of MAP kinases and NF-κB in macrophages. First, activation of c-Jun N-terminal kinase (JNK), p38, and extracellular signal-regulated kinase (ERK) induced by MALP-2 was profoundly impaired in *IRAK-4*$^{-/-}$ as well as *IRAK-4*$^{KN/KN}$ macrophages (Fig. 6, C–E). These results indicate that IRAK-4 activity is critical for the activation of MAP kinases in the TLR signaling.

We analyzed activation of NF-κB. Phosphorylation and degradation of IκBα were also severely impaired in *IRAK-4*$^{-/-}$ and *IRAK-4*$^{KN/KN}$ macrophages (Fig. 7, A and B). MALP-2–induced phosphorylation of NF-κB p65 was not observed in *IRAK-4*$^{-/-}$ and *IRAK-4*$^{KN/KN}$ macrophages (Fig. 7 C). Nevertheless, an electrophoretic mobility shift assay (EMSA) revealed that the NF-κB–DNA binding activity was clearly induced even in the absence of IRAK-4, although the activation was ~10 min delayed compared with wild-type cells (Fig. 7 D). Consistent with our previous study, *MyD88*$^{-/-}$ macrophages failed to induce NF-κB–DNA binding activity in response to MALP-2 (Fig. S3, available at http://www.jem.org/cgi/content/full/jem.20061523/DC1; reference 26). These results indicate that TLR2 activates a MyD88-dependent and IRAK-4–independent signaling pathway leading to the activation of NF-κB. To assess the subunits of the NF-κB complexes observed in response to MALP-2 stimulation, we performed supershift assays using anti-p65 or anti-p50 Ab and nuclear extracts from macrophages stimulated with MALP-2 for 40 min (Fig. 7 E). In wild-type and IRAK-4–mutated cells, the bands were supershifted with anti-p65 and anti-p50 Ab, suggesting that the NF-κB complex is mainly composed of p65/p50 heterodimers in both wild-type and IRAK-4–mutated cells. These findings indicate that TLR2 activates a MyD88-dependent and IRAK-4–independent signaling pathway leading to the

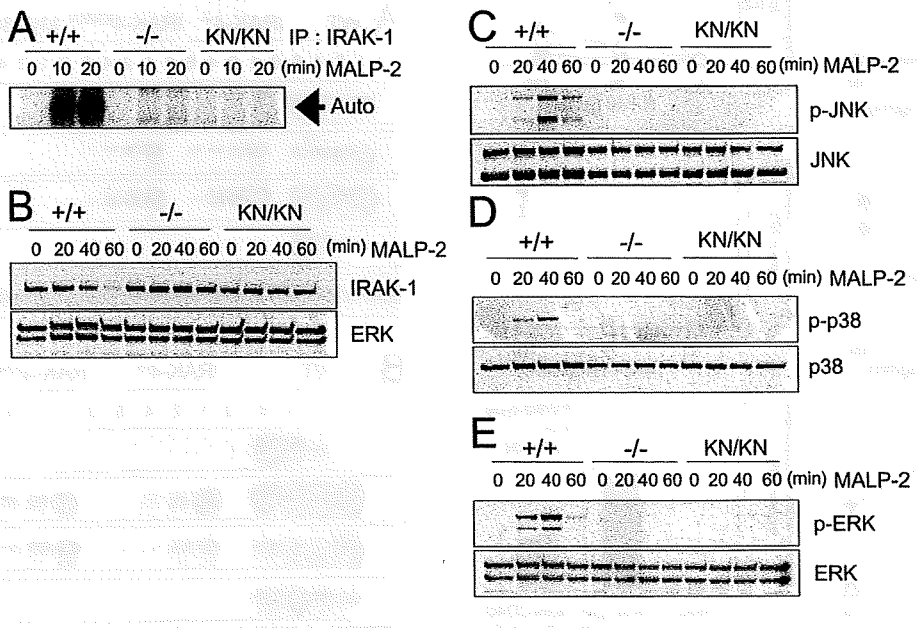

Figure 6. IRAK-4 is critical for TLR-mediated activation of IRAK-1 and MAP kinases. (A) In vitro kinase assay for IRAK-1 activation. Peritoneal macrophages were stimulated with 10 ng/ml MALP-2 for the indicated periods. The cell lysates were prepared and immunoprecipitated with anti-IRAK-1 Ab, and the kinase activity of IRAK-1 was measured by in vitro kinase assay. The data shown are representative of three independent experiments. Auto, autophosphorylation. (B) Immunoblot analysis for the change in IRAK-1 expression in response to MALP-2 stimulation. Peritoneal macrophages from wild-type, *IRAK-4*$^{-/-}$, and *IRAK-4*$^{KN/KN}$ mice were stimulated with MALP-2 for the indicated periods. Whole cell lysates were subject to immunoblot analysis using anti-IRAK-1. ERK1/2 levels are shown as loading control. (C–E) Macrophages from wild-type, *IRAK-4*$^{-/-}$, and *IRAK-4*$^{KN/KN}$ mice were stimulated with MALP-2 for the indicated periods, and whole cell lysates were subject to immunoblot analysis using anti-phospho-JNK (C), anti-phospho-P38 (D), and anti-phospho-ERK (E). The blots of JNK, p38, and ERK are shown as loading controls. Similar results were obtained in three independent experiments.

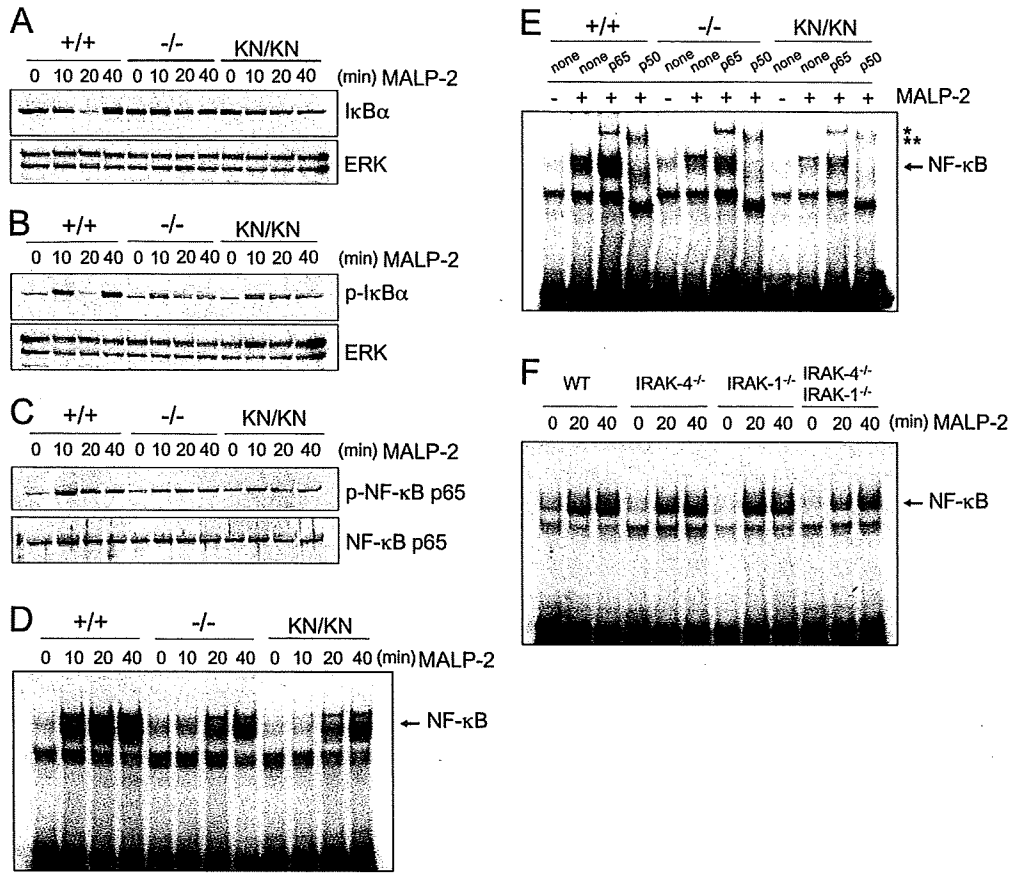

Figure 7. IRAK-4–independent activation of NF-κB in TLR2 signaling. (A–C) Macrophages from wild-type, *IRAK-4*$^{-/-}$, and *IRAK-4*$^{KN/KN}$ mice were stimulated with MALP-2 for the indicated periods. Whole cell lysates were subject to immunoblot analysis using anti-IκBα (A), anti-phospho-IκBα (B), and anti-phospho-NF-κB p65 Abs (C). The blots of ERK1/2 and NF-κB p65 are shown as loading controls. The data are representative of three independent experiments. (D) Wild-type, *IRAK-4*$^{-/-}$, and *IRAK-4*$^{KN/KN}$ macrophages were stimulated with 10 ng/ml MALP-2 for the indicated periods. Nuclear extracts were then prepared, and NF-κB–DNA binding activity was determined by EMSA using an NF-κB–specific probe. (E) Nuclear extracts from macrophages stimulated with MALP-2 for 40 min were incubated with Abs specific to NF-κB p65 and p50 before addition of NF-κB probe. The single and double asterisks indicate the supershifts induced by Ab to p65 and p50, respectively. (F) IRAK-1/IRAK-4–independent activation of NF-κB in response to TLR stimulation. Wild-type, *IRAK-4*$^{-/-}$, *IRAK-1*$^{-/-}$, and *IRAK-4*$^{-/-}$*IRAK-1*$^{-/-}$ doubly deficient macrophages were stimulated with 10 ng/ml MALP-2 for the indicated periods. NF-κB–DNA binding activity was determined by EMSA.

activation of NF-κB. Stimulation with R-848 and CpG-DNA also induced NF-κB activation in an IRAK-4–independent manner without degrading IκBα (Fig. S4). When IRAK-4–mutated cells were stimulated with LPS, degradation of IκBα as well as NF-κB–DNA binding was delayed as observed in *MyD88*$^{-/-}$ macrophages (Fig. S4). These data indicate that the IRAK- 4–independent pathway is activated downstream of various TLRs.

Activation of NF-κB in the IRAK-1–independent and IRAK-4–dependent signaling pathway

It was revealed that the death domain of MyD88 is responsible for triggering downstream signaling cascades. Given that only IRAK-4 and -1 have intrinsic kinase activity, it was hypothesized that IRAK-4 and -1 function redundantly in activating NF-κB. Therefore, we generated IRAK-1/IRAK-4 doubly deficient mice and examined the response to MALP-2. As shown in Fig. 7 F, the activation of NF-κB–DNA binding activity was induced even in the absence of both IRAK-1 and -4. Furthermore, TLR2-induced TNF-α gene induction was still observed in *IRAK-1*$^{-/-}$*IRAK-4*$^{-/-}$ macrophages (unpublished data). Thus, IRAK-1– and IRAK-4–independent mechanisms are responsible for the signaling pathway leading to the activation of NF-κB.

Normal TCR responses in *IRAK-4*$^{-/-}$ and *IRAK-4*$^{KN/KN}$ T cells

A recent study has shown that deficiency in IRAK- 4 results in the impaired responses to TCR stimulation (18). IRAK-4 interacts with ZAP-70 in the cells and regulates TCR-mediated activation of NF-κB. We then analyzed responses of *IRAK-4*$^{KN/KN}$ mice to TCR stimulation. Surprisingly, proliferation of purified T cells in response to either immobilized or soluble anti-CD3 was not impaired in either *IRAK-4*$^{-/-}$ or *IRAK-4*$^{KN/KN}$ mice compared with wild-type mice

(Fig. 8 A and Fig. S5, available at http://www.jem.org/cgi/content/full/jem.20061523/DC1). In addition, production of IL-2 in response to TCR stimulation was not impaired in T cells from these mice (Fig. 8 B). Furthermore, wild-type, *IRAK-4*$^{-/-}$, and *IRAK-4*$^{KN/KN}$ T cells have equivalent ability to proliferate in response to allogenic DCs either untreated or treated with various TLR ligands, including MALP-2, LPS, and CpG-DNA (Fig. 8 C). Moreover, TCR-mediated activation of NF-κB as well as MAP kinases was also not altered between wild-type, *IRAK-4*$^{-/-}$, and *IRAK-4*$^{KN/KN}$ T cells (Fig. 8, D and E). We investigated whether IRAK-4 was involved in adaptive T cell responses in vivo. Wild-type and *IRAK-4*$^{-/-}$ mice were infected with lymphocytic choriomeningitis virus (LCMV). Splenocytes were prepared 8 d after infection, and induction of LCMV-specific CD8$^+$ T cells was analyzed by tetramer staining. As shown in Fig. 9 A, LCMV-specific CD8$^+$ T cells were induced both in wild-type and *IRAK-4*$^{-/-}$ mice in a similar manner after infection. Similarly, wild-type and *IRAK-4*$^{-/-}$ mice induced comparable ex vivo CTL responses as determined in a ^{51}Cr release assay (Fig. 9 B). These results indicate that IRAK-4 is not involved in the TCR signaling leading to the activation of NF-κB as well as T cell responses in vivo.

DISCUSSION

In the present study, we analyzed the role of IRAK-4 activity in vivo by generating mice with knockin mutation KK213AA and with null mutation. In agreement with previous papers, *IRAK-4*$^{-/-}$ macrophages showed severe defects in TLR-mediated cytokine responses (14, 15). Although the expression of IRAK-4 protein was slightly lower than wild-type cells, *IRAK-4*$^{KN/KN}$ macrophages also showed profound defects in the responses to various TLR ligands to the same extent as *IRAK-4*$^{-/-}$ cells. These results clearly indicate that the kinase activity of IRAK-4 is essential for the function of IRAK-4 in vivo. Previous in vitro studies implicated that the IRAK family members could activate NF-κB and inflammatory responses even in the absence of their kinase activity (19, 20). In the case of IRAK-4, one group has shown that the mutant IRAK-4 (KK213AA) restored IL-1β responsiveness (22), and the other group reported that the same mutation could restore the response only partially (23). It has been shown that expression of kinase-inactive IRAK-1 could also restore IL-1β–induced NF-κB activation. It may be possible that overexpressed IRAK-4 behaved differently compared with the physiological expression. In the physiological level of expression, the kinase activity of IRAK-4 is critical for its function. So far IRAK-4 substrates responsible for the signaling

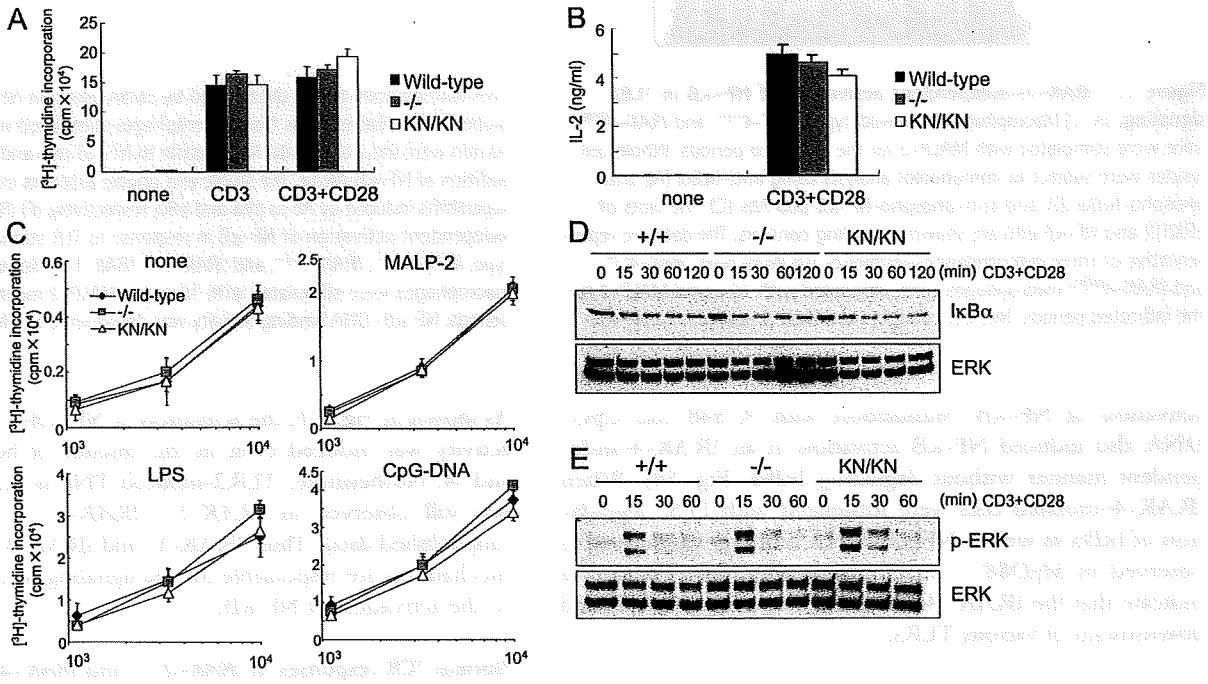

Figure 8. IRAK-4 is dispensable for TCR signaling. (A) Splenic T cells from wild-type, *IRAK-4*$^{-/-}$, and *IRAK-4*$^{KN/KN}$ mice were stimulated with immobilized (plate-bound) anti-CD3 (5 μg/ml) alone or anti-CD3 (5 μg/ml) plus anti-CD28 (2 μg/ml) for 48 h. The cells were pulsed with 1 μCi [3H]thymidine for the last 16 h. [3H]thymidine incorporation was measured by a β-scintillation counter. (B) Splenic T cells were stimulated with 5 μg/ml anti-CD3 plus 2 μg/ml anti-CD28 for 72 h. IL-2 concentrations in the culture supernatant were measured by ELISA. (C) Allogenic activity of wild-type, *IRAK-4*$^{-/-}$, and *IRAK-4*$^{KN/KN}$ T cells. T cells from indicated mice were mixed with bone-marrow DCs from BALB/c mice stimulated with MALP-2, LPS, and CpG-DNA. (D) Normal activation of NF-κB in response to TCR in *IRAK-4*$^{-/-}$ and *IRAK-4*$^{KN/KN}$ mice. The cell lysates from cells stimulated with plate-bound anti-CD3 plus anti-CD28 were immunoblotted with anti-IκBα. ERK1/2 levels are shown as loading control. (E) Normal activation of ERK in *IRAK-4*$^{-/-}$ and *IRAK-4*$^{KN/KN}$ mice. Wild-type, *IRAK-4*$^{-/-}$, and *IRAK-4*$^{KN/KN}$ T cells were stimulated with plate-bound anti-CD3 plus anti-CD28, and the cell lysates were immunoblotted with anti-phospho-ERK. ERK1/2 levels are shown as loading control.